JOURNAL OF PETROLOGY | VOLUME 46 | NUMBER 5 | PAGES 859–891 | 2005 | doi:10.1093/petrology/egi003

Contemporaneous Trachyandesitic and Calc-alkaline Volcanism of the Huerto Andesite, San Juan Volcanic Field, Colorado, USA

FLEURICE PARAT[1]*, MICHAEL A. DUNGAN[1] AND PETER W. LIPMAN[2]

[1]DÉPT. MINÉRALOGIE, UNIVERSITÉ DE GENÈVE, RUE DES MARAÎCHERS 13, 1211 GENÈVE 4, SWITZERLAND

[2]US GEOLOGICAL SURVEY, 345 MIDDLEFIELD ROAD, MENLO PARK, CA 94025, USA

RECEIVED APRIL 21, 2004; ACCEPTED DECEMBER 1, 2004
ADVANCE ACCESS PUBLICATION JANUARY 21, 2005

Locally, voluminous andesitic volcanism both preceded and followed large eruptions of silicic ash-flow tuff from many calderas in the San Juan volcanic field. The most voluminous post-collapse lava suite of the central San Juan caldera cluster is the 28 Ma Huerto Andesite, a diverse assemblage erupted from at least 5–6 volcanic centres that were active around the southern margins of the La Garita caldera shortly after eruption of the Fish Canyon Tuff. These andesitic centres are inferred, in part, to represent eruptions of magma that ponded and differentiated within the crust below the La Garita caldera, thereby providing the thermal energy necessary for rejuvenation and remobilization of the Fish Canyon magma body. The multiple Huerto eruptive centres produced two magmatic series that differ in phenocryst mineralogy (hydrous vs anhydrous assemblages), whole-rock major and trace element chemistry and isotopic compositions. Hornblende-bearing lavas from three volcanic centres located close to the southeastern margin of the La Garita caldera (Eagle Mountain–Fourmile Creek, West Fork of the San Juan River, Table Mountain) define a high-K calc-alkaline series (57–65 wt % SiO_2) that is oxidized, hydrous and sulphur rich. Trachyandesitic lavas from widely separated centres at Baldy Mountain–Red Lake (western margin), Sugarloaf Mountain (southern margin) and Ribbon Mesa (20 km east of the La Garita caldera) are mutually indistinguishable (55–61 wt % SiO_2); they are characterized by higher and more variable concentrations of alkalis and many incompatible trace elements (e.g. Zr, Nb, heavy rare earth elements), and they contain anhydrous phenocryst assemblages (including olivine). These mildly alkaline magmas were less water rich and oxidized than the hornblende-bearing calc-alkaline suite. The same distinctions characterize the voluminous precaldera andesitic lavas of the Conejos Formation, indicating that these contrasting suites are long-term manifestations of San Juan volcanism. The favoured model for their origin involves contrasting ascent paths and differentiation histories through crustal columns with different thermal and density gradients. Magmas ascending into the main focus of the La Garita caldera were impeded, and they evolved at greater depths, retaining more of their primary volatile load. This model is supported by systematic differences in isotopic compositions suggestive of crust–magma interactions with contrasting lithologies.

KEY WORDS: *alkaline; calc-alkaline; petrogenesis; episodic magmatism; Fish Canyon system*

INTRODUCTION

Tertiary volcanic rocks of intermediate to silicic composition occur widely in western North America; many have been interpreted as the products of continental-arc volcanism related to subduction along the western margin of the North American plate (e.g. Lipman *et al.*, 1972; Coney & Reynolds, 1977). Although the magma chemistry of the Oligocene San Juan volcanic field is broadly consistent with an arc setting and regional extension did not begin until after San Juan volcanism ceased, the large distance from the Oligocene continental margin (>700 km) is anomalous with respect to modern convergent margin arcs. To better constrain the petrological evolution of such magmatic systems, voluminous ash-flow tuffs of the central San Juan volcanic field have been studied extensively (e.g. Ratté & Steven, 1967;

*Corresponding author. Present address: Institut für Mineralogie, Universität Hannover, Callinstrasse 3, D-30167 Hannover, Germany. Telephone: (49) (0)511 762 5517. Fax: (49) (0)511 762 3045. E-mail: f.parat@mineralogie.uni-hannover.de

Lipman *et al.*, 1978; Whitney & Stormer, 1985; Whitney *et al.*, 1988; Johnson & Rutherford, 1989; Riciputi, 1991; Lipman *et al.*, 1997), whereas less attention has been paid to the contemporaneous andesitic lavas. Although the eruptive volume of these relatively mafic lavas is smaller than the voluminous ignimbrites, their presence is significant because mafic magmas may be parental to, or provide the heat sources responsible for the generation of, felsic magmas and they may record chemical contributions from mantle and crustal reservoirs during magma generation and differentiation.

The Huerto Andesite is a diverse assemblage of proximal lavas and distal laharic breccias from several eruptive centres around the southern margin of the La Garita caldera, the source of the 28 Ma Fish Canyon Tuff (Fig. 1). Huerto volcanism is broadly typical of the dominantly andesitic background magmatism that occurred within and around many San Juan calderas during repose periods between large silicic ash-flow eruptions. Emplaced shortly after the Fish Canyon Tuff, Huerto lavas probably represent continued eruptions from the assumed magmatic source of heat and volatiles that induced the rejuvenation of the Fish Canyon system (Bachmann *et al.*, 2002). The Huerto Andesite includes two contrasting but broadly contemporaneous differentiation series: (1) olivine-bearing lavas, primarily basaltic trachyandesite and trachyandesite (Askren *et al.*, 1991); (2) hornblende-bearing high-K calc-alkaline mafic andesitic to dacitic dykes and lavas. These two series of the Huerto Andesite exhibit distinctions in whole-rock chemistry and mineralogy comparable with contrasting members of the Conejos Formation (35–29 Ma precaldera regional lavas).

We investigated both the olivine- and hornblende-bearing lavas of the Huerto Andesite to: (1) document the diverse mineral assemblages and ranges in major element, trace element and isotopic compositions of eruptive products; (2) derive constraints from phenocryst compositions on the pre-eruptive temperatures, oxygen fugacities, pressures and water contents so as to evaluate the petrological processes that produced the spectrum of compositions; (3) determine whether contrasting lavas in the Huerto Andesite and Conejos Formation arose primarily as a result of differences in parental magma composition and/or were contaminated under different conditions by contrasting crustal components; (4) determine whether the andesites could be parental to felsic ash-flow tuffs; (5) assess the role of Huerto Andesite magmas in rejuvenating and remobilizing young, partly solidified subcaldera plutons that led to eruption of the Fish Canyon Tuff; (6) evaluate the source signatures and crustal imprints of Huerto magmas so as to better constrain the magmatism of the San Juan volcanic field.

GEOLOGY AND ERUPTIVE HISTORY OF THE SAN JUAN VOLCANIC FIELD

The San Juan volcanic field (*c.* 25 000 km^2, 40 000 km^3; Larsen & Cross, 1956; Lipman *et al.*, 1970; Steven & Lipman, 1976) is among the largest erosional remnants of the widespread intermediate to silicic magmatism that characterized the North American Cordillera during mid-Tertiary time (Lipman *et al.*, 1972). Volcanism in the San Juan volcanic field began about 35 Ma with the eruption of the precaldera Conejos Formation, a thick (>1 km) sequence of lavas and volcanic breccias, dominated by pyroxene- and hornblende-bearing andesite, with lesser amounts of dacite and minor rhyolite (Larsen & Cross, 1956; Lipman *et al.*, 1978; Colucci *et al.*, 1991), that were erupted from widely scattered volcanic centres. About 29 Ma, activity shifted to eruptions of large volumes of dacitic and rhyolitic ash-flow tuffs plus intracaldera lavas. At least 17 major ash-flow tuffs were erupted from a minimum of 14 calderas, and at least 60% of the total volume of ash-flow tuffs in the field was erupted from the nine calderas of the central caldera cluster (Lipman, 1975, 2000). At about 26 Ma, the character of volcanism changed to bimodal eruptions of basalt and rhyolite (Hinsdale Formation) associated with the initial extension of the Rio Grande Rift.

Overview of the central San Juan volcanic field

Following early ash-flow volcanism concentrated in the Platoro and western caldera complexes (Fig. 1), explosive volcanic activity converged on the central San Juan region (Steven & Lipman, 1976; Lipman, 2000). Between 28·3 and 26·7 Ma, nine major ash-flow tuffs (overall, >8000 km^3) were erupted from at least nine calderas (Fig. 1). Caldera-related volcanism of the central cluster began with the Masonic Park Tuff (28·3 Ma) from a source that was entirely buried by the subsequent eruption of the La Garita caldera during the Fish Canyon Tuff eruption (28·0 Ma; Fig. 1). Four ash-flow sheets subsequently erupted from calderas nested within the central and southern segments of the La Garita caldera, and lavas interlayered between these ash-flow tuffs erupted within or just outside the margins of the caldera cluster (e.g. Sheep Mountain, Huerto and Bristol Head Andesites, Fig. 1). Finally, the last stages of central San Juan volcanism (27·0–26·7 Ma) consisted of the eruption of multiple tuffs and lavas from the San Luis caldera complex nested within the NW La Garita caldera and from the more centrally located Creede caldera (Fig. 1).

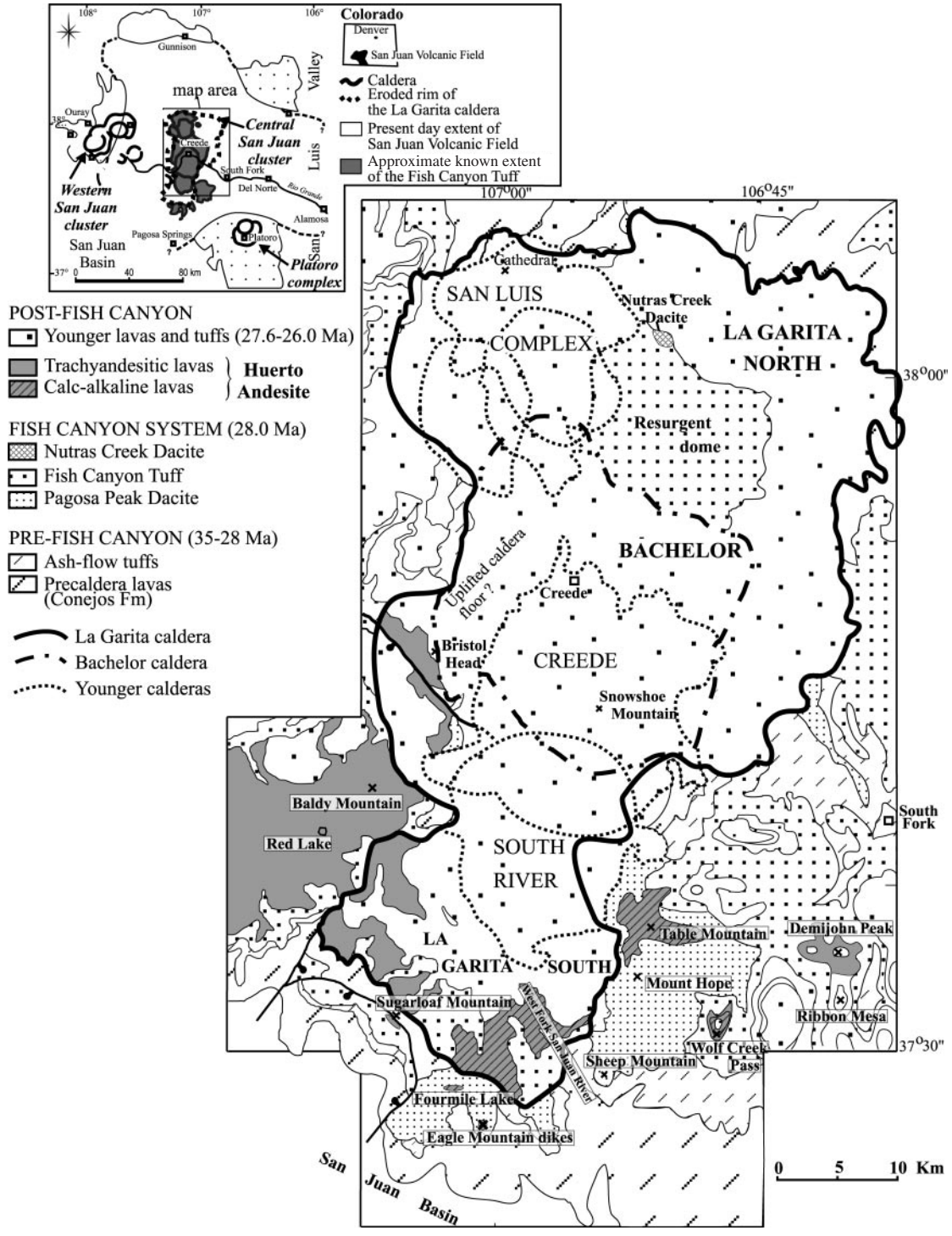

Fig. 1. Generalized geological map of the central San Juan volcanic field, Colorado [after Lipman *et al.* (1997)].

The Huerto Andesite

The Huerto Andesite comprises more than 200 km^3 of lava flows and associated volcanic breccias. Its age of 28 Ma is bracketed stratigraphically by the Fish Canyon (28·0 Ma) and Carpenter Ridge Tuffs (27·6 Ma), which were erupted respectively from the La Garita and Bachelor calderas (Lipman *et al.*, 1970; Steven *et al.*, 1974; Lipman, 2000). Erosional remnants of the Huerto

Andesite are widely scattered (>50 km NE–SW), within and adjacent to the southern segment of the La Garita caldera. Thick successions (>750 m) of relatively thin flows and associated laharic breccias are present over large areas to the west of the caldera, whereas scattered thinner accumulations occur in and around the southern and eastern caldera margins. These scattered occurrences must be the remnants of at least 5–6 eruptive centres. This widely dispersed distribution and the local involvement of the Huerto Andesite in faulting that predates the Carpenter Ridge Tuff (Lipman, 2000) suggest that the Huerto Andesite is an immediately postcaldera phase of activity from the broadly defined Fish Canyon magmatic system, comparable with postcaldera andesitic volcanism associated with several other San Juan ash-flow calderas (Steven & Lipman, 1976).

The various Huerto Andesite eruptive centres produced two magma series, olivine-bearing andesites (Askren *et al.*, 1991) and hornblende-bearing andesites, on the basis of the mutually exclusive presence of either mineral as a stable, crystallizing phase. The two series have been observed in the same stratigraphic section only locally, along the West Fork of the San Juan River (WFSJR) and at Wolf Creek Pass (Fig. 1), where olivine-bearing lavas at the base of the Huerto sequence directly underlie hornblende-bearing lavas. Thus, at least locally, olivine-bearing lavas erupted before hornblende-bearing lavas. The regional distribution of these contrasting Huerto lithologies remains incompletely mapped; for example, a major area of hornblende-bearing Huerto lavas near Table Mountain (Fig. 1) was misinterpreted as part of a post-Huerto sequence until recently (Lipman, 2000).

Three sequences of olivine-bearing lavas within the broad arcuate outcrop area of the Huerto Andesite have been sampled at (1) a thick section on Baldy Mountain near the western margin of the La Garita caldera, (2) thin widespread flows in the Ribbon Mesa area to the east of the southeastern margin, and (3) a small erosional remnant near Sugarloaf Mountain in the south margin (Fig. 1). All three lie outside the La Garita caldera and are up to 35 km distant from each other, suggesting that these lavas represent the products of at least three volcanic centres. Lavas from all three centres are basaltic trachyandesites to trachyandesites with similar mineral assemblages and textures, suggesting that the parental magma compositions and pre-eruptive equilibration conditions were closely comparable over a wide geographical area. The locations and morphologies of the vent areas for these edifices remain poorly constrained. Dykes crop out on the north slope of Baldy Mountain and to the south; red oxidized cinders appear to mark a vent at Red Lake (Fig. 1); and two intrusions of plagioclase-phyric trachyandesite to the east, near the margin of La Garita caldera, probably mark additional vents (Lipman, 2004). In the Ribbon Mesa area, a few dykes have been mapped, but no central vent or obvious constructional edifice is preserved. Little can be reconstructed from present observations concerning the source of the Sugarloaf Mountain sequence.

Hornblende-bearing andesites occur in several discontinuous outcrop areas but their distribution is even more closely associated with the southern La Garita caldera. Lavas exposed in the West Fork of the San Juan River (WFSJR), within the southern La Garita caldera, closely resemble lavas from Table Mountain [not sampled for this study; analyses have been given by Riciputi (1991), Yager *et al.* (1991) and Christe (2001)], which lies just outside the caldera (Fig. 1). At Eagle Mountain on the east side of Fourmile Creek and along the ridge crest at the head of Fourmile Creek, just outside the southern margin of the La Garita caldera, hornblende-bearing dykes intrude the Pagosa Peak Dacite (Bachmann *et al.*, 2000). Source volcanic centres for the hornblende-bearing lavas also remain poorly defined. A thick dyke (~150 m) at Eagle Mountain may be the central intrusion of a stratovolcano that produced at least some of the WFSJR sequence; the Table Mountain lavas probably represent the surviving east flank of a volcano that is now largely buried within the younger South River caldera (Fig. 1).

Chemical discrimination criteria and terminology

Differences in alkali concentrations, alkali–lime index and FeO*/MgO ratio are used in conjunction with mineralogical distinctions to discriminate between the two magma series, which are characterized by divergent major-element evolution trends. Lavas that contain only anhydrous phenocryst phases (plagioclase + olivine + augite ± hypersthene) have higher total alkali contents and alkali–lime indices at a given SiO_2 content (Fig. 2). They form a series from alkalic–calcic basaltic trachyandesite to silicic trachyandesite. Neither K-feldspar nor biotite has been observed. As these alkali-rich olivine-bearing lavas define an elevated trend for FeO*/MgO vs SiO_2, intermediate between a true tholeiitic differentiation series and a typical calc-alkaline series (Fig. 2c; Miyashiro, 1974), they are referred to as trachyandesitic lavas to emphasize their high alkali contents and alkali–lime index. Hornblende-bearing lavas span the compositional range from mafic andesite to dacite (Fig. 2). On the basis of their alkali–lime index, total alkali contents and FeO*/MgO ratios (Fig. 2), these hornblende-bearing lavas define a high-K calc-alkaline series, which is further subdivided, according to geographical distribution, mineralogy and contrasting geochemistry and isotopic signatures into the Fourmile Creek dykes and the calc-alkaline lavas from the WFSJR.

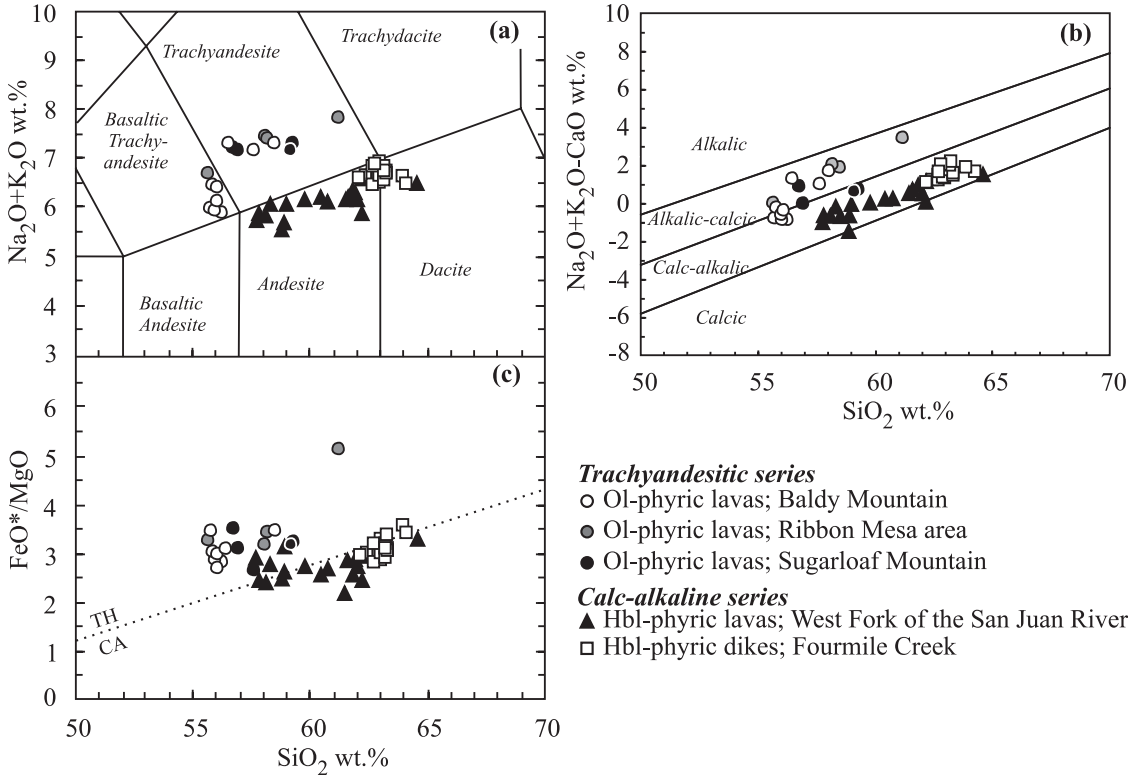

Fig. 2. (a) Total alkalis ($Na_2O + K_2O$) (anhydrous, e.g. normalized to 100% volatile free) vs wt % SiO_2 (anhydrous), after Le Bas *et al.* (1986); (b) alkali–lime index (anhydrous), after Peacock (1931); (c) FeO*/MgO (anhydrous) vs wt % SiO_2 (anhydrous). Definition of tholeiitic (TH) vs calc-alkaline (CA) andesites after Miyashiro (1974) for the Huerto lavas and dykes. Ol, olivine; Hbl, hornblende.

PETROLOGY

Petrography and modal mineralogy

Trachyandesitic lavas from all three outcrop areas contain plagioclase, olivine, clinopyroxene and orthopyroxene, plus accessory ilmenite, titanomagnetite, apatite and pyrrhotite. Lavas are either porphyritic or seriate-textured. Porphyritic lavas with 16–20 vol. % phenocrysts and microphenocrysts (Fig. 3a) are characterized by fine-grained groundmasses of plagioclase + pyroxenes + oxides, whereas highly crystalline seriate-textured lavas with 37–65 vol. % phenocrysts and microphenocrysts (Fig. 3b) contain abundant altered dark brown glass plus microlites of plagioclase + pyroxenes + oxides. In all samples, plagioclase phenocrysts are volumetrically dominant (11–47 vol. %); olivine, augite and hypersthene have similar modal abundances (<1–7 vol. %) (Fig. 4). Apatite is rare and occurs only in the groundmass and as inclusions in pyroxene phenocrysts. Pyrrhotite is present as inclusions in Fe–Ti oxides and in the groundmass. Mineral compositions do not vary systematically with texture, outcrop location, or whole-rock composition.

The calc-alkaline lavas contain phenocrysts of plagioclase, hornblende and clinopyroxene ± orthopyroxene, plus accessory ilmenite, titanomagnetite, apatite, pyrrhotite ± anhydrite in glass-rich groundmasses, along with many randomly oriented small crystals of plagioclase (<50 μm), pyroxene and titanomagnetite (Fig. 3c and d). Total phenocryst plus microphenocryst abundances do not vary systematically from andesite to dacite (40–60 vol. %; Fig. 4). All lavas contain phenocrysts of amphibole (1–14 vol. %) and plagioclase (30–40 vol. %). Augite and amphibole decrease (6–1 vol. % and 10–1 vol. %, respectively), whereas hypersthene increases (2–7 vol. %) from mafic andesite to dacite in the WFSJR (Fig. 4). Apatite occurs as inclusions in every phenocryst phase and in the groundmass. Titanomagnetite is ubiquitous; ferrian ilmenite occurs only in dacite. Pyrrhotite and pyrite are more common in dacitic lavas, where they occur as inclusions in phenocrysts. The Fourmile Creek dykes (Fig. 3d) are distinguished from WFSJR lavas by: (1) higher modal abundance of amphibole (10–14 vol. %); (2) sparse hypersthene (<2 vol. %); (3) the presence of anhydrite as inclusions in amphibole.

Mineral chemistry and phase equilibria

Plagioclase

Plagioclase is the most abundant phenocryst and groundmass phase in all the Huerto lavas. Phenocryst textures

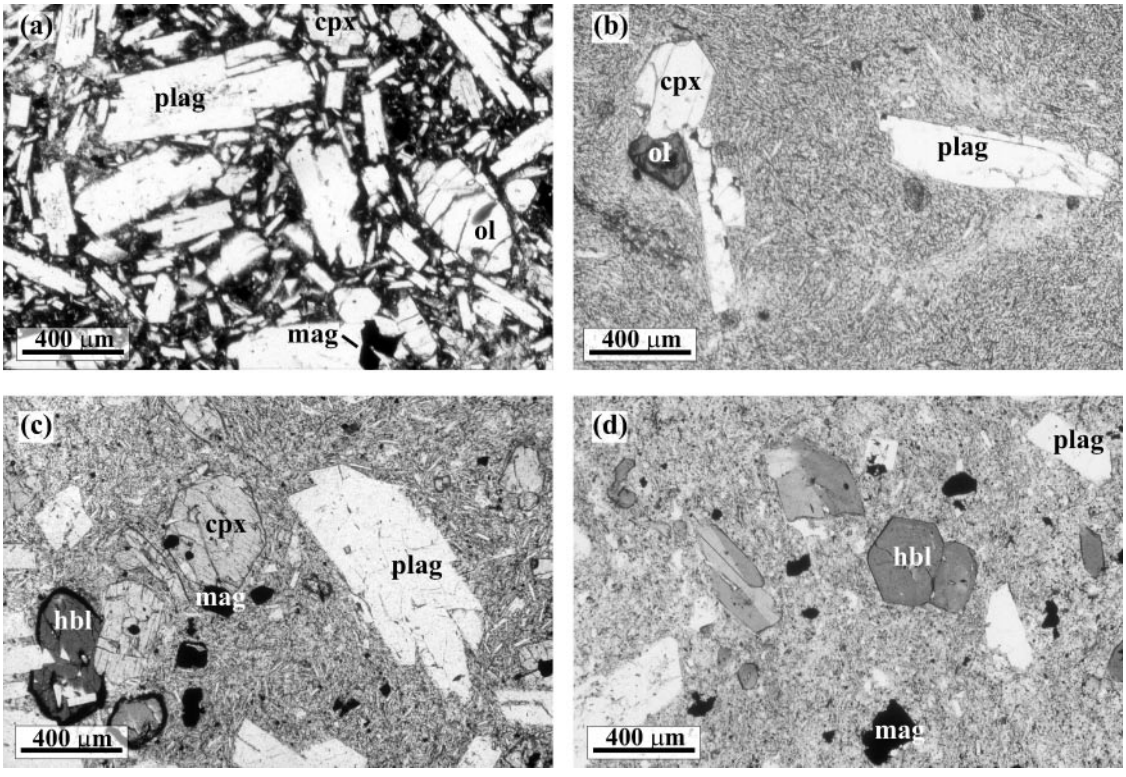

Fig. 3. Photomicrographs of representative trachyandesitic lavas (a, b) and calc-alkaline lavas (c, d) of the Huerto Andesite. (a) Seriate basaltic trachyandesite (HA34); (b) porphyritic trachyandesite (HA31); (c) calc-alkaline andesite from the West Fork of the San Juan River (WFSJR) (HA9); (d) Fourmile Creek (FC) calc-alkaline andesite (DA4). plag, plagioclase; ol, olivine; cpx, clinopyroxene; hbl, hornblende; mag, magnetite. This figure can be viewed in colour on *Journal of Petrology* online.

and compositions differ among the two series (Fig. 5; Table 1). Basaltic trachyandesites and trachyandesites contain abundant (11–47 vol. %), large tabular plagioclase phenocrysts (up to 7 mm) [platy plagioclase phenocrysts of Lipman (1975)]; some rounded, embayed and skeletal morphologies are similar to those described by Hibbard (1981) for rapidly grown plagioclase phenocrysts in supercooled, plagioclase-saturated magma. Individual phenocrysts are mostly normally zoned ($An_{79–36}$, maximum range for many samples), characterized by unusually rapid increases in Or with decreasing An content (to Or_9 at An_{36}). Plagioclase phenocrysts in calc-alkaline lavas are smaller, with maximum diameters <2·5 mm. In most samples, plagioclase phenocrysts are euhedral, normally zoned with a maximum range for many samples from $An_{68}Or_{0·2}$ to $An_{40}Or_4$ (Fig. 5) and contain inclusions of apatite needles and altered glass. In WFSJR lavas, some euhedral phenocrysts are normally zoned from An-rich cores of An_{82} to rims of An_{75}. Groundmass microlites are similar in composition to phenocryst rims ($An_{60}Or_2$ to $An_{40}Or_4$). The Fourmile Creek dykes contain euhedral, weakly zoned plagioclase ($An_{55}Or_1$ to $An_{32}Or_4$). Differences in plagioclase compositions between the two Huerto magma series are comparable with those observed for contrasting Conejos lavas (Colucci *et al.*, 1991), where large Or-rich plagioclase phenocrysts occur in the mildly alkaline lavas (Rock Creek member; no hydrous phases) and Or-poor plagioclase characterizes the calc-alkaline lavas (Horseshoe Mountain member; hornblende in mafic andesites).

Pyroxenes

Hypersthene and augite are present in both trachyandesitic and calc-alkaline lavas. Modal abundances of pyroxenes vary widely among the trachyandesitic lavas (Fig. 4) and augite and hypersthene occur both as large euhedral phenocrysts (up to 2 mm) and as sparse euhedral microphenocrysts (0·1–0·25 mm). Augite is the most abundant mafic mineral in the calc-alkaline andesites, whereas hornblende dominates in mafic andesite and hypersthene dominates in dacite (Fig. 4). Hypersthene is rare in Fourmile Creek samples.

Pyroxenes in trachyandesites have higher Ti and lower Na and Mn contents (Table 1) than those in the calc-alkaline lavas, but the main difference in the pyroxene compositions of the two series is that calcium contents in augite are lower in trachyandesitic lavas (16–20 wt %) than

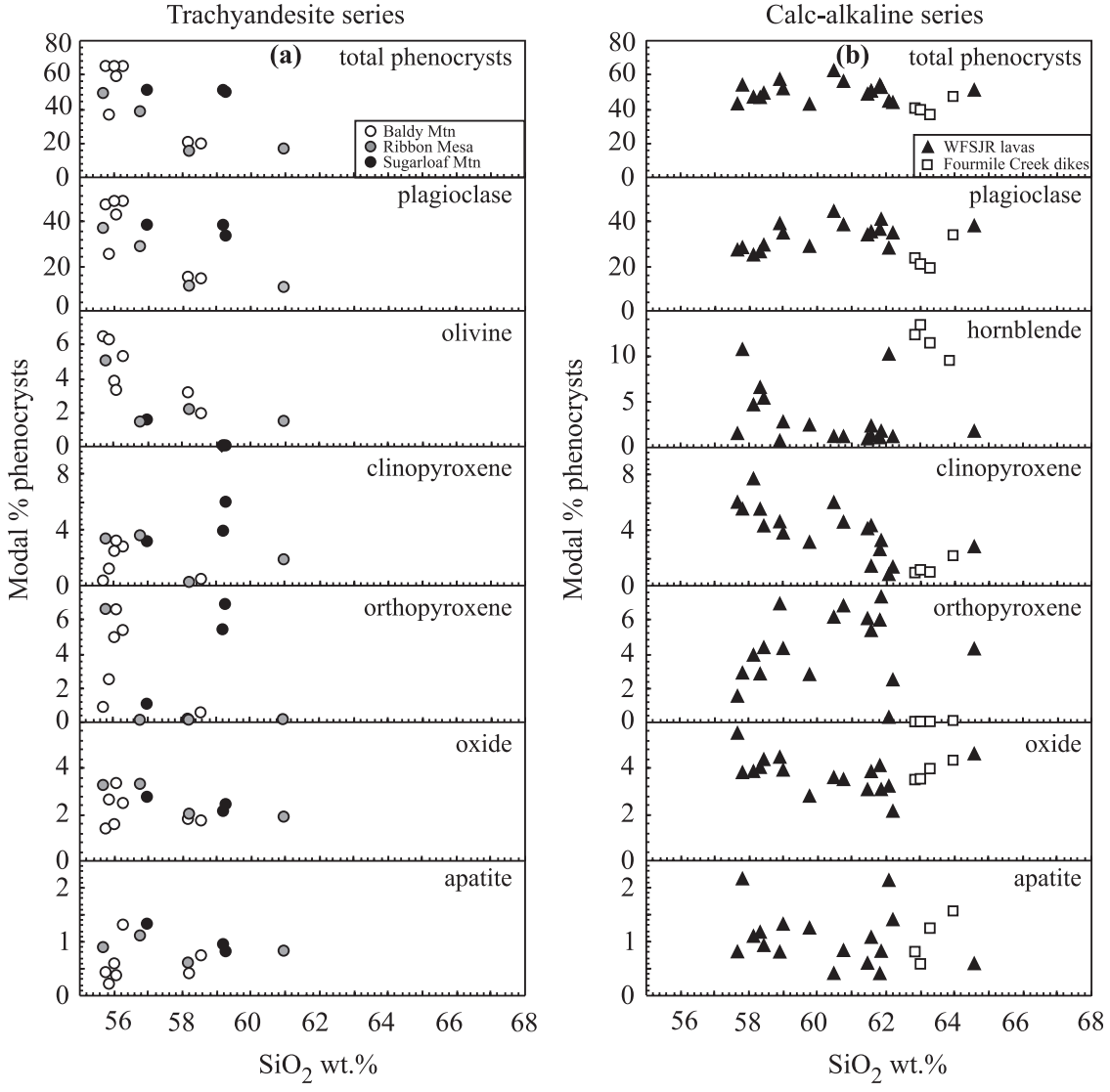

Fig. 4. Modal abundances of phenocrysts (>50 μm) in lavas and dykes of the Huerto Andesite vs wt % SiO_2 (anhydrous). (a) Trachyandesitic lavas; (b) calc-alkaline lavas and dykes.

in calc-alkaline lavas (18–22 wt %), suggesting a higher crystallization temperature (Lindsley, 1983) and/or lower water contents in the trachyandesitic lavas (Gaetani *et al.*, 1993). In both trachyandesitic and calc-alkaline samples, $Mg/(Mg + Fe_t)$ is higher in clinopyroxene than in orthopyroxene (Table 1) and textural associations are consistent with early crystallization of clinopyroxene, followed by orthopyroxene. $Mg/(Mg + Fe_t)$ ratios of augite do not vary from basaltic trachyandesites to trachyandesites, suggesting that augite in trachyandesites may have been inherited from less evolved magmas. In calc-alkaline lavas, augite has $Mg/(Mg + Fe_t)$ ranging from 0·77 to 0·62 in mafic andesite to dacite. Exchange coefficients for the distribution of Fe_t and Mg between augite and andesitic liquids range between 0·3 and 0·4, close to those determined by experiments on calc-alkaline lavas (Grove *et al.*, 1982; Sisson & Grove, 1993; Pichavant *et al.*, 2002), suggesting that augite is a near-liquidus phase in equilibrium with calc-alkaline whole-rock compositions.

Olivine

Sparse olivine grains occur as euhedral phenocrysts in basaltic trachyandesite (5–6 vol. %, 0·4–1·3 mm) and trachyandesite (1–2 vol. %, 0·2–0·4 mm). In seriate-textured basaltic trachyandesites, olivine is resorbed (Fig. 3a) and contains plagioclase (An_{60}) plus glass inclusions; in porphyritic lavas olivine is replaced by calcite and iddingsite (Fig. 3b). Olivine also occurs as inclusions in titanomagnetite in basaltic trachyandesites.

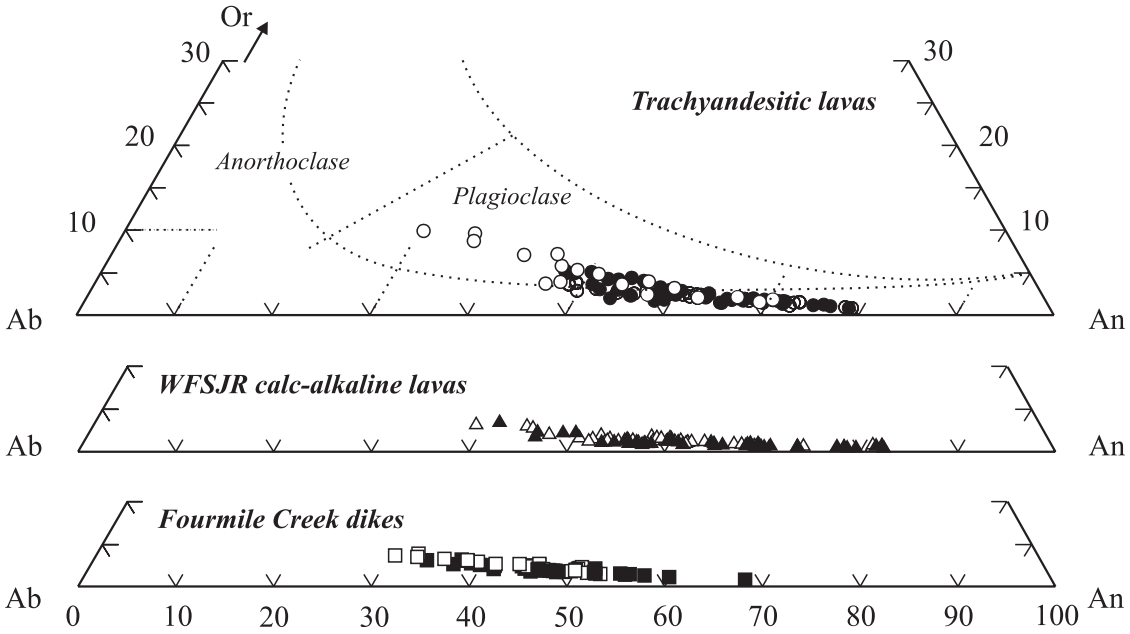

Fig. 5. Portion of the feldspar ternary diagram showing cores (filled symbols) and rims (open symbols) of plagioclase phenocrysts in lavas and dykes of the Huerto Andesite. WFSJR, West Fork of the San Juan River. Nomenclature from Smith & Brown (1988).

Olivine phenocrysts are weakly zoned (Fo_{68} to Fo_{64}), except in the outermost rims (5–10 μm) where forsterite content decreases from Fo_{64} to Fo_{55} (Table 1). The exchange coefficient calculated for the distribution of Fe and Mg between olivine phenocryst cores and liquids similar in composition to the host whole rock is about 0·37, close to the equilibrium value ($K_d = 0·33$) obtained by Sisson & Grove (1993) for basaltic compositions, suggesting that olivine is a near-liquidus phase. However, $Mg/(Mg + Fe^{2+})$ in most olivine cores ($Fo_{68–53}$) is lower than in clinopyroxenes, for which $Mg/(Mg + Fe^{2+})$ is 0·81–0·66, and similar to those of orthopyroxene, suggesting either that clinopyroxene is the first magnesian phase to crystallize followed by olivine + orthopyroxene, in accord with experiments on high-alumina basalt at low pressure ($P < 3$ kbar) and 2 wt % water (Baker & Eggler, 1987), or that near-liquidus Fo-rich olivine has been physically segregated.

Amphibole

The foremost mineralogical distinction between the two Huerto series is the presence of amphibole (up to 5 mm) and the absence of olivine in the calc-alkaline lavas. The Fourmile Creek dykes contain abundant unoxidized green amphibole without reaction rims (~10–14 vol. %, Figs 3d and 4); the calc-alkaline lavas have variable abundances (1–10 vol. %) of oxidized amphibole with reaction rims of pyroxene, oxides and ± plagioclase (Figs 3c and 4). The amphibole breakdown reaction is absent where the amphibole is in contact with another crystalline phase; comparable textural indications of mineral disequilibrium are not observed for other phases.

The amphiboles have compositions ranging from magnesiohornblende to magnesiohastingsite, with $(Ca)_B > 0·5$ and $0·35 < (Na + K)_A < 0·7$ (Leake *et al.*, 1997). Amphibole phenocrysts are normally zoned; $Mg/(Mg + Fe_t)$ in cores ranges from 0·70 to 0·54 and silica and alumina contents range from 46 to 41 wt % and 9 to 13 wt % respectively in both mafic andesite and dacite (Table 1). Halogen contents (Cl and F) are low, except for amphibole rims in dacitic lavas from the WFSJR, where the fluorine content is up to 1 wt % (HA18, Table 1). Increases in F content toward amphibole rims in dacite indicate that hydroxyl ions are replaced by fluorine and thus amphiboles crystallized from a melt with lower water content and/or higher F content (Table 1). The Al/Si ratios of the Huerto amphiboles do not vary significantly from mafic andesite to dacite but the total range is large in one sample (Al/Si = 0·24–0·38). The highest Al/Si ratios are slightly high compared with predicted ratios based on the Al/Si exchange coefficients determined by Sisson & Grove (1993) for melt and amphibole, suggesting that Huerto amphiboles crystallized primarily from less evolved andesites. $Mg/(Mg + Fe_t)$ ratios of Huerto amphiboles are constant from mafic andesite to andesite and values are close to those determined by experiments (Sisson & Grove, 1993). The $Mg/(Mg + Fe_t)$ ratios of amphibole may reflect a combination of crystallization at variable oxygen fugacity (high Fe^{3+}) or variable sulphur

Table 1: Representative electron microprobe analyses of silicate and oxide minerals of the Huerto Andesite

	Plagioclase							
	Trachyandesitic lavas				Calc-alkaline lavas and dykes			
	Basaltic trachyandesite		Trachyandesite		Fourmile Creek andesite		WFSJR andesite	
	HA37 core	HA37 rim	HA28 core	HA28 rim	DA4 core	DA4 rim	HA18 core	HA18 rim
wt %								
SiO_2	53·20	54·53	53·81	57·17	54·02	57·38	52·17	56·08
Al_2O_3	28·90	27·80	29·33	27·10	29·03	27·26	30·59	27·30
Fe_2O_3*	0·83	0·80	0·67	0·65	0·31	0·23	0·55	0·64
MgO	0·11	0·08	0·06	0·07	0·02	0·03	0·02	0·07
CaO	12·03	11·01	11·95	9·56	11·43	9·27	13·15	9·74
BaO	0·10	0·06	0·01	0·08	0·02	0·02	0·03	0·05
Na_2O	4·51	5·18	4·36	5·45	5·04	6·24	3·90	5·77
K_2O	0·42	0·61	0·60	1·06	0·24	0·37	0·24	0·40
Total	100·09	100·07	100·79	101·14	100·11	100·81	100·64	100·06
Ab mol. %	39·44	44·40	38·40	47·67	43·80	53·76	34·39	50·56
An mol. %	58·14	52·16	58·15	46·22	54·80	44·14	64·23	47·16
Or mol. %	2·42	3·44	3·45	6·11	1·40	2·10	1·37	2·28

	Pyroxenes										
	Trachyandesitic lavas					Calc-alkaline lavas and dykes					
	Basaltic trachyandesite			Trachyandesite		Fourmile Creek andesite		WFSJR basaltic andesite		Andesite	
	HA37 Aug-core	HA37 Aug-rim	HA37 Opx-core	HA31 Aug-core	HA31 Aug-rim	DA4 Aug-core	EMA3 Opx-core	HA14 Aug-core	HA14 Opx-core	HA18 Aug-core	HA18 Opx-core
wt %											
SiO_2	51·33	51·71	51·88	51·94	51·31	52·25	51·29	52·56	52·32	51·67	53·31
TiO_2	0·60	0·61	0·31	0·48	0·63	0·33	0·11	0·29	0·24	0·40	0·18
Al_2O_3	1·82	1·85	1·00	1·49	2·05	1·32	1·00	1·47	1·34	2·62	0·67
FeO†	10·42	10·37	21·36	9·85	9·80	8·67	23·16	8·77	20·43	9·48	20·45
MnO	0·42	0·46	0·61	0·36	0·29	0·50	1·00	0·59	0·91	0·66	1·13
MgO	15·26	14·74	22·06	15·46	14·99	15·02	21·18	15·67	23·40	15·29	22·93
CaO	19·21	19·55	2·03	19·91	19·88	21·09	1·01	20·25	1·38	20·02	1·52
Na_2O	0·28	0·32	0·03	0·28	0·28	0·35	0·01	0·33	0·01	0·32	0·03
Total	99·34	99·61	99·29	99·77	99·23	99·53	98·76	99·94	100·04	100·46	100·24
En	43·41	42·28	61·52	43·68	42·89	42·51	59·70	44·16	64·34	43·35	63·45
Fs	17·31	17·43	34·40	15·90	16·22	14·58	38·24	14·81	32·94	15·62	33·53
Wo	39·28	40·29	4·08	40·42	40·89	42·91	2·06	41·03	2·72	41·03	3·02
Mg-no.	0·72	0·72	0·65	0·74	0·73	0·76	0·62	0·76	0·67	0·74	0·67

Table 1: Continued

	Hornblende										Olivine				
	Fourmile Creek andesite				WFSJR basaltic andesite		Andesite		Dacite			Basaltic trachyandesite		Trachyandesite	
	DA10 core	DA10 rim	HA2 core	HA2 rim	HA14 core	HA14 rim	HA6 core	HA6 rim	HA18 core	HA18 rim		HA34 core	HA34 rim	HA37 core	HA37 rim
wt %											*wt %*				
SiO_2	41·63	41·13	46·08	45·68	42·36	43·22	44·08	45·00	42·45	42·05	SiO_2	37·02	35·51	35·92	36·17
TiO_2	2·63	2·67	2·17	2·08	2·39	2·43	2·15	2·65	2·42	2·47	TiO_2	0·02	0·06	0·01	0·03
Al_2O_3	12·57	12·57	8·33	9·08	11·88	11·50	11·43	9·22	12·15	12·16	Al_2O_3	0·04	0·03	0·01	0·03
FeO†	14·52	14·38	12·81	14·23	13·29	13·89	14·01	12·41	13·01	13·69	FeO†	30·84	37·11	33·11	32·99
MnO	0·22	0·23	0·31	0·31	0·21	0·37	0·29	0·34	0·13	0·17	MnO	0·67	0·74	0·82	0·82
MgO	11·99	12·06	14·73	13·62	13·63	13·28	13·29	14·34	13·70	13·44	MgO	32·33	26·38	30·00	30·10
CaO	11·76	11·92	11·68	11·18	11·53	11·35	11·33	11·62	11·68	11·66	CaO	0·19	0·31	0·21	0·23
Na_2O	2·48	2·45	1·97	1·99	2·31	2·22	2·40	2·17	2·19	2·31	Cr_2O_3	0·00	0·01	n.a.	n.a.
K_2O	0·80	0·79	0·53	0·69	0·86	0·75	0·67	0·64	0·75	0·78	NiO	0·06	0·04	n.a.	n.a.
F	0·10	0·02	0·24	0·22	0·14	0·19	0·26	0·28	0·19	1·07	Total	101·17	100·14	100·09	100·37
Cl	0·04	0·04	0·06	0·07	0·01	0·02	0·03	0·03	0·01	0·03					
Total	98·75	98·25	98·92	99·14	98·60	99·20	99·94	98·68	98·68	99·83	Fo	65·14	55·90	61·76	61·93
											Fa	34·86	44·10	38·24	38·07
Mg-no.	0·59	0·59	0·67	0·63	0·65	0·63	0·63	0·67	0·65	0·64					

	Oxides								Apatite						
	Trachyandesitic lavas				Calc-alkaline lavas and dykes				Trachyandesitic lavas			Calc-alkaline lavas and dykes			
	Basaltic trachyandesite		Trachyandesite		Fourmile Creek andesite		WFSJR andesite		Basaltic trachyandesite	Trachyandesite		Fourmile Creek andesite		WFSJR andesite	
	HA37 Mag	HA37 Ilm	HA31 Mag	HA31 Ilm	DA4 Mag	DA4 Ilm	HA18 Mag	HA18 Ilm	HA37	HA31	HA29	DA10	HA2	HA14	HA9
wt %									*wt %*						
SiO_2	0·17	0·08	0·09	0·11	0·14	0·05	0·11	0·11	SiO_2	0·13	0·21	0·26	0·37	0·35	0·28	0·25
TiO_2	14·19	46·31	15·29	48·21	6·84	40·28	11·13	47·12	FeO†	0·68	0·26	0·82	0·92	0·79	0·48	0·96
Al_2O_3	0·75	0·06	3·87	0·08	0·85	0·12	1·29	0·04	CaO	54·95	55·34	54·25	54·63	54·35	55·01	52·73
FeO†	78·21	50·13	73·61	49·47	84·04	55·09	80·88	46·84	Ce_2O_3	0·17	0·10	0·26	0·10	0·25	0·10	0·19
MgO	0·32	0·67	1·54	0·46	0·58	1·12	0·29	0·65	Na_2O	0·05	0·04	0·09	0·36	0·28	0·20	0·07
MnO	0·56	0·79	0·69	0·79	0·53	0·74	0·73	1·59	P_2O_5	42·16	42·00	41·69	42·01	41·42	41·45	41·09
V_2O_3	0·00	0·00	0·00	0·00	0·00	0·00	0·00	0·00	SO_3	0·01	0·07	0·04	1·01	0·58	0·59	0·16
Cr_2O_3	0·00	0·00	0·00	0·00	0·00	0·01	0·02	0·00	MnO	0·05	0·06	0·12	0·09	0·18	0·20	0·17
NiO	0·00	0·00	0·00	0·02	0·03	0·00	0·05	0·02	SrO	0·00	0·00	0·00	0·00	0·00	0·02	0·00
ZnO	0·18	0·02	0·04	0·03	0·24	0·00	0·07	0·08	F	3·65	3·91	4·08	2·55	2·62	2·35	2·77
Total	94·39	98·06	95·13	99·17	93·24	97·40	94·57	96·44	Cl	0·22	0·21	0·33	0·33	0·67	0·38	0·46
									Total	102·08	102·20	101·94	102·37	101·48	101·05	98·84
X_{ulv}	0·42		0·49		0·20		0·33		O=F,Cl	1·59	1·69	1·79	1·15	1·25	1·08	1·27
X_{ilm}		0·89		0·90		0·76		0·92	Total	100·49	100·51	100·15	101·22	100·23	99·98	97·57
									Cl/F	0·06	0·03	0·04	0·07	0·14	0·09	0·09

*Total iron as Fe^{3+}.
†Total iron as Fe^{2+}.
Ab, An and Or calculated according to Deer *et al*. (1992); En, Fo, Wo calculated according to Morimoto *et al*. (1988); Fo, Fa calculated according to Deer *et al*. (1992). Aug, augite; Opx, orthopyroxene; Mg-number = $Mg/(Mg + Fe_t)$; n.a., not analysed.

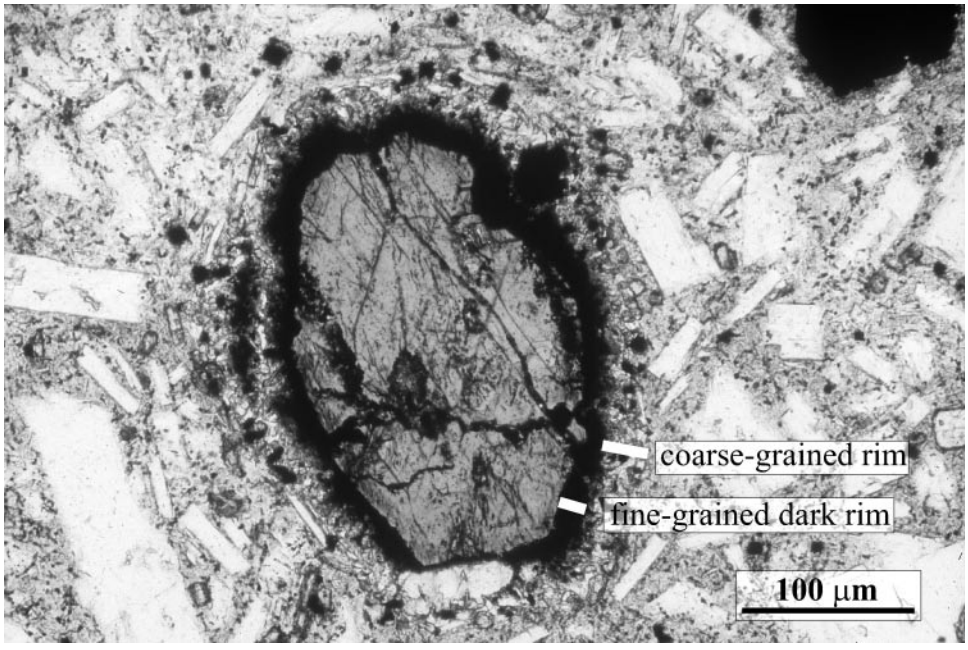

Fig. 6. Transmitted light image of an amphibole with coarse-grained rim of plagioclase + pyroxene + magnetite (~40 μm) surrounding a fine-grained dark rim of oxide + pyroxene (~20 μm) from a dacitic lava (West Fork of the San Juan River, HA17). This figure can be viewed in colour on *Journal of Petrology* online.

fugacity (Moore & Carmichael, 1998; Scaillet & Evans, 1999) and crystallization from a less evolved magma as suggested by the Al/Si ratios. The lower $Mg/(Mg + Fe_t)$ ratios of amphiboles compared with pyroxenes suggest that pyroxenes primarily crystallized before amphiboles.

Two types of amphibole breakdown rims occur in andesitic and dacitic lavas from the WFSJR: (1) fine-grained dark rims (<40 μm) consisting of iron oxides and pyroxenes (Fig. 3c); (2) more coarse-grained rims (50–100 μm) of plagioclase, pyroxenes and oxides (Fig. 6) surrounding the fine-grained dark rims. The breakdown reaction rim is absent where the amphibole is in contact with another crystalline phase. Fine-grained amphibole breakdown rims occur in mafic andesite where amphibole represents 6–10 vol. % of phenocrysts; the coarse-grained type surrounding the fine-grained rims occurs in andesite and dacite where amphibole is rare (1–3 vol. %).

Fe–Ti oxides

Unexsolved, compositionally homogeneous titanomagnetite and ferrian ilmenite coexist in most trachyandesitic and calc-alkaline samples (Fig. 7, Table 1). Coexisting pairs were established where possible by analysing adjoining grains and all putative pairs were screened according to the partitioning test of Bacon & Hirschmann (1988). Magnetite (up to 1 mm) commonly contains inclusions of apatite, pyrrhotite, pyrite, ilmenite and altered glass; ilmenite is less abundant, smaller and free of inclusions. Concentrations of Cr_2O_3 (<0·2 wt %), V_2O_5 (<0·9 wt %), ZnO (<0·5 wt %) and NiO (<0·1 wt %) in both oxide series are negligible and Al_2O_3 contents are 1–5 wt %. Titanomagnetite compositions in trachyandesitic lavas (X_{usp} = 0·30–0·64; Fig. 7) extend to higher ulvöspinel contents than do those of the calc-alkaline lavas (X_{usp} = 0·17–0·38). Titanomagnetite occurs as inclusions in silicate phases and in the groundmass of trachyandesitic lavas, but high-titanium ilmenite (X_{ilm} = 0·83–0·94) is present only in the glassy groundmass. In the WFSJR calc-alkaline lavas, ilmenite occurs only in dacite where there are two compositional populations. One occurs as inclusions in hornblende (X_{ilm} = 0·86) with magnetite (X_{usp} = 0·27) and the other (X_{ilm} = 0·92) is restricted to the groundmass (equilibrium magnetite X_{usp} = 0·33). In the Fourmile Creek dykes, two populations of ilmenite are also present: (1) an anomalously Ti-poor population (X_{ilm} = 0·56–0·61), which occurs both as inclusions in hornblende and in the groundmass, without coexisting equilibrium magnetite; (2) a more Ti-rich population, which is present only in the groundmass (X_{ilm} = 0·76–0·80) and which coexists with titanomagnetite (X_{usp} = 0·25).

Apatite

Apatite occurs as rare euhedral crystals (up to 0·3 mm) in the groundmass of all trachyandesites and as inclusions in the pyroxenes of silicic trachyandesites, suggesting that it

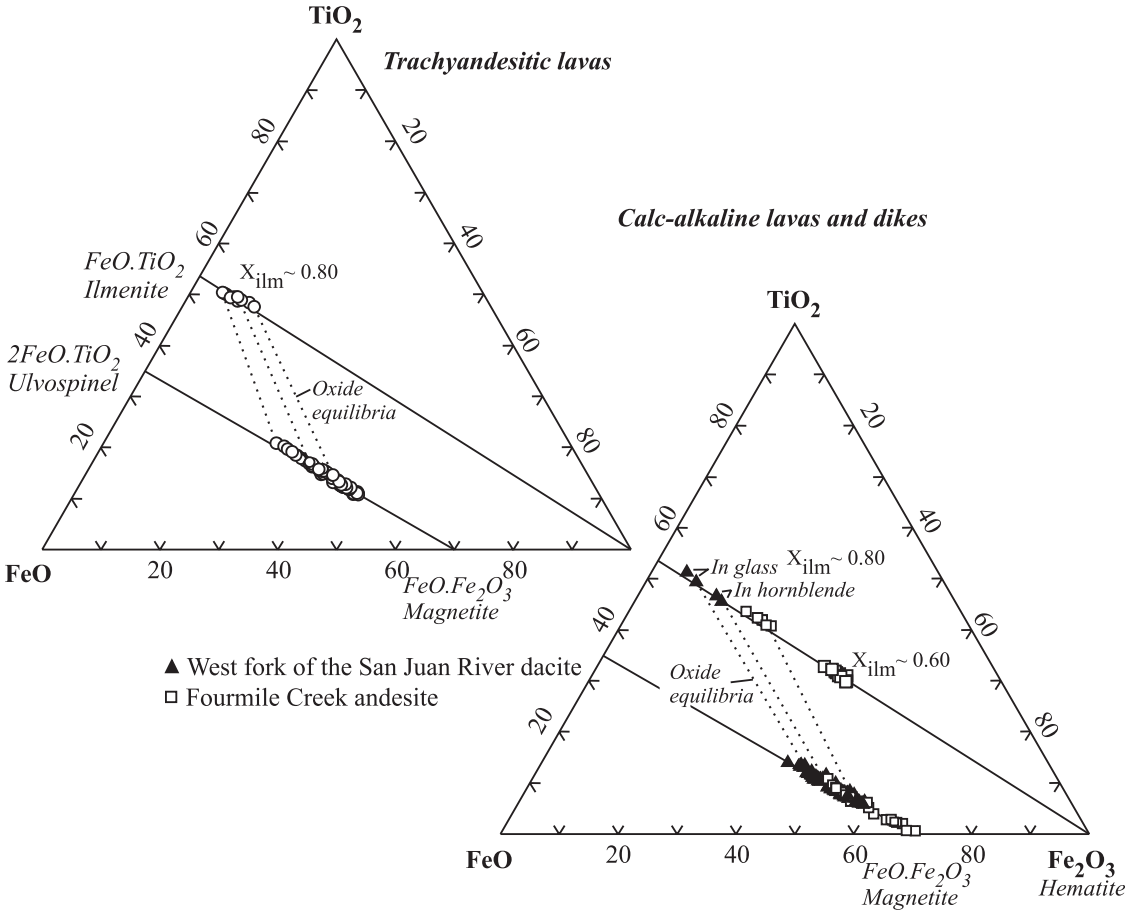

Fig. 7. Titanomagnetite and ilmenite compositions represented as molar proportions in the FeO–Fe_2O_3–TiO_2 ternary. Oxide equilibria based on the partitioning test of Bacon & Hirschmann (1988). Recalculations of FeO, Fe_2O_3 and mineral formulae after Stormer (1983).

crystallized relatively late. Apatites have low Na_2O (<0·1 wt %), MnO (<0·16 wt %), sulphur (<0·09 wt %) and chlorine (<0·3 wt %) contents, but high fluorine contents (up to 4·8 wt %; Cl/F = 0·02–0·05), suggesting that the host magma was relatively fluorine rich, but chlorine and sulphate poor (Fig. 8, Table 1).

Apatite (50–250 mm) is more abundant in calc-alkaline lavas and dykes, even though P_2O_5 is generally lower in these rocks (Table 2). Apatite occurs as free crystals or as acicular inclusions in all phenocryst phases. These textural relationships indicate that apatite began crystallizing early. Apatite in the calc-alkaline rocks has a higher sodium content (up to 0·5 wt % Na_2O) and higher MnO content (up to 0·25 wt %) than in the trachyandesitic lavas (Table 1). Apatites in the calc-alkaline lavas also have relatively high sulphur and water contents (Fig. 8). Apatites from the Fourmile Creek andesite have the highest sulphate contents (0·04–1·28 wt % SO_3). These data have been used to estimate the sulphur content in the melt at about 900 ppm (Parat *et al.*, 2002). Apatite is OH rich and has a high Cl/F ratio ranging from 0·04 to 0·24 (Fig. 8). Sulphate contents are not well correlated with halogen contents, but apatites in calc-alkaline lavas have lower sulphate and chlorine contents than in the Fourmile Creek dykes.

Sulphate and sulphide

Sparse pyrrhotite and pyrite occur in both series. Pyrrhotite is relatively abundant in calc-alkaline rocks and rare in the trachyandesites, whereas pyrite is more common in the latter. Round to oval blebs of pyrrhotite and pyrite, 5–40 μm in diameter, form inclusions in plagioclase, pyroxenes and especially in titanomagnetite in both series, and occur in hornblende and apatite in calc-alkaline lavas and dykes. Microprobe analyses indicate a small range for Fe/S (N_{FeS} = 0·93–0·98) and show no detectable metal substitution for Fe (Table 1). Pyrite is also present and was probably formed from oxidation of pyrrhotite at temperatures below ~740°C (Carroll & Rutherford, 1987).

Anhydrite has been identified only in the Fourmile Creek dykes (Parat *et al.*, 2002). It occurs as small

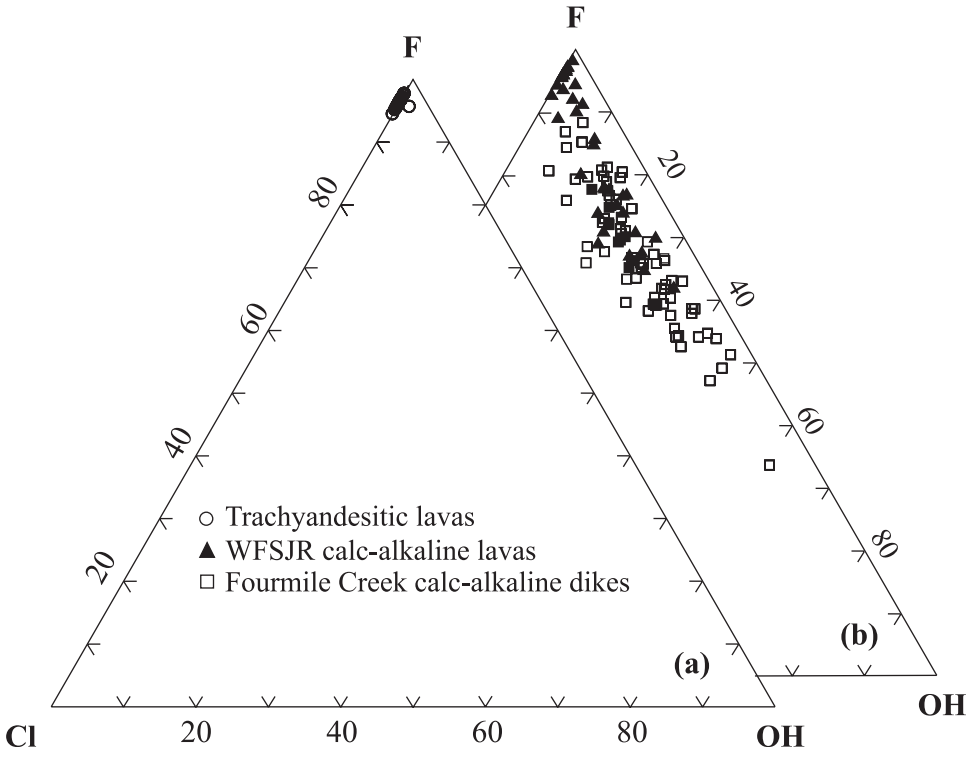

Fig. 8. Halogen and OH variations in apatite from lavas and dykes of the Huerto Andesite. (a) Trachyandesitic lavas; (b) calc-alkaline lavas and dykes. WFSJR, West Fork of the San Juan River.

inclusions (~30 μm) in hornblende. Both anhydrite and pyrrhotite are present as inclusions in phenocrysts, indicating that they crystallized well before eruption and that sulphur existed as both oxidized (S^{6+}) and reduced (S^{2-}) species in the melt.

ESTIMATES OF MAGMATIC INTENSIVE PARAMETERS AND WATER CONTENTS

Temperature and oxygen fugacity

Temperatures and oxygen fugacities, determined with the Ghiorso & Sack (1991) oxide geothermometer, are in general agreement with independent constraints derived from contrasting silicate phenocryst assemblages (anhydrous mineralogy vs hornblende-bearing) and the presence of S-bearing phases. The olivine-bearing trachyandesitic series records higher temperatures and less oxidized conditions [QFM (quartz–fayalite–magnetite) to NNO (nickel–nickel oxide)] than the hornblende-bearing calc-alkaline series (NNO to NNO + 1·3) (Fig. 9). Although evolved trachyandesitic lavas tend to cluster near the QFM buffer, the hotter and the more mafic sample is more oxidized (HA37: NNO, 992 ± 30°C). Oxide inclusions in hornblende from a calc-alkaline dacite (HA18) give a temperature and an oxygen fugacity of 800 ± 30°C and $\log fO_2 = \text{NNO} + 0{\cdot}5$, whereas oxide microphenocrysts in the groundmass indicate $T = 740 \pm 30$°C and $\log fO_2 = \text{QFM}$. If both pairs of oxides are valid recorders of oxidation states, a decrease in oxygen fugacity with falling temperature is also indicated for the WFSJR lavas (Fig. 9). A temperature of 890 ± 30°C and an oxygen fugacity of NNO + 1·3 calculated from coexisting oxides in Fourmile Creek dykes (samples DA 4 and EMA3) is consistent with the presence of magmatic anhydrite, given that the experimentally determined limit for anhydrite + pyrrhotite stability is at 1–1·5 log units above NNO (Carroll & Rutherford, 1988). The elevated oxygen fugacity in the amphibole-bearing Fourmile Creek andesite, relative to trachyandesite, is consistent with higher water contents in the calc-alkaline magmas (Eggler & Burnham, 1973).

Temperatures of coexisting pyroxenes obtained with the QUILF geothermometer (Lindsley & Frost, 1992) are higher than those calculated from coexisting oxides, but yield comparable differences between the hotter trachyandesitic lavas (1113 ± 28°C; sample HA32) and the cooler hornblende-bearing magmas (1007 ± 15°C for mafic andesite HA14, 1004 ± 47°C for dacite HA18 from WFSJR; 895 ± 19°C for Fourmile Creek andesite

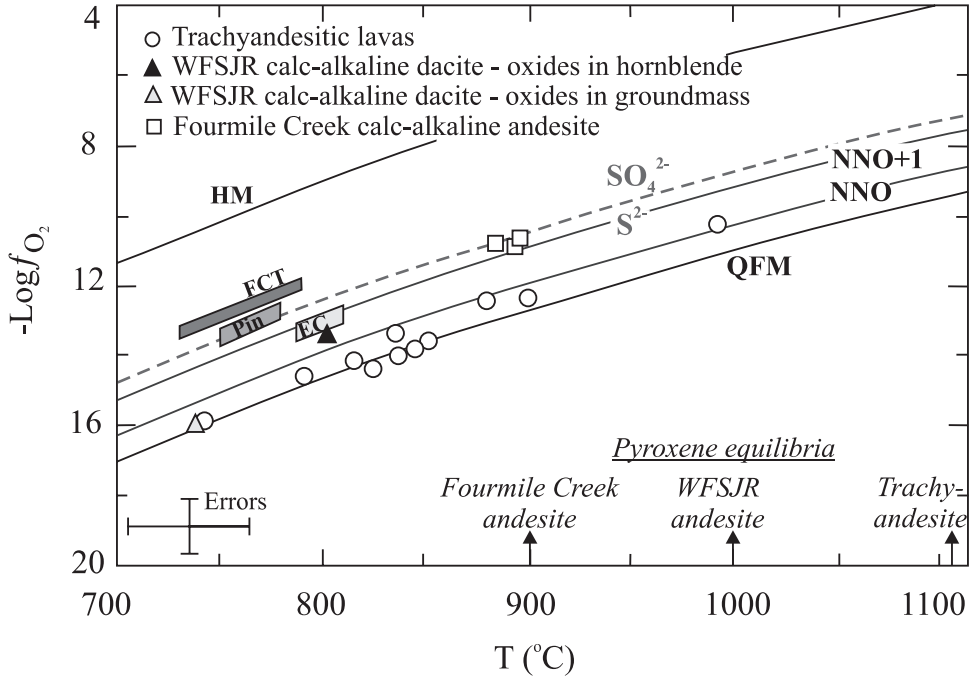

Fig. 9. T–fO_2 conditions calculated from the composition of coexisting magnetite and ilmenite solid solutions in the Huerto Andesite using the Ghiorso & Sack (1991) geothermometer and pyroxene equilibrium temperature from Lindsley & Frost (1992) (see text for estimated standard error). Pin, Pinatubo dacite from Scaillet & Evans (1999); EC, El Chichón from Luhr (1990); FCT, Fish Canyon tuff (Johnson & Rutherford, 1989; Evans & Scaillet, 1997); WFSJR, West Fork of the San Juan River.

EMA3). Similarly, apatite saturation temperatures estimated from whole-rock P_2O_5 contents (Harrison & Watson, 1984) define a range for trachyandesitic lavas from 1028°C in mafic basaltic trachyandesite (HA35) to 904°C in silicic trachyandesite (HA31) and a narrower interval for the calc-alkaline magmas (~960–900°C).

Total pressure and water content

At present, no mineral geobarometer exists to determine total lithostatic pressure during crystallization of Huerto Andesite magmas. The association of the deposits of the Huerto Andesite with a large caldera implies crystallization in the upper crust (2–4 kbar), but this is a loose constraint. However, the anhydrous mineral assemblage olivine–plagioclase–clinopyroxene–orthopyroxene in the trachyandesitic series can place constraints on liquidus water content and pressure by comparison with experimental investigations. Experiments by Moore & Carmichael (1998) on calc-alkaline andesite from Colima reproduced similar mineral assemblages and phase proportions at 1·3 kbar, 1000°C and 4–3·5 wt % H_2O. For Fourmile Creek dykes, the abundant hornblende (14 vol. %) and sparse orthopyroxene may constrain the pressure at ~2–4 kbar and H_2O >5·5 wt % for $T = 1000$°C (Moore & Carmichael, 1998; Scaillet & Evans, 1999) or $P = 1·6$ kbar, $T = 900$°C and 4·6 wt % H_2O (Rutherford & Hill, 1993).

Although it is not possible to precisely define the water content of the Huerto magmas, the reaction rims on amphibole in WFSJR calc-alkaline lavas are consistent with water loss during magmatic differentiation. Two mechanisms may explain the breakdown rims around amphiboles: (1) loss of water in the magma storage region; or (2) loss of water from the coexisting melt during magma ascent (Rutherford & Hill, 1993). The lack of an independent estimate for the depth of the magma chamber does not allow discrimination between these two alternatives.

WHOLE-ROCK CHEMICAL COMPOSITIONS OF LAVAS AND DYKES

A significant feature of the genesis and evolution of Oligocene magmas in the voluminous San Juan volcanic field is the absence of erupted basalt and the rarity of even mafic basaltic andesite (<55 wt % SiO_2 or >3·5 wt % MgO). In light of isotopic evidence for large crustal contributions to San Juan magmatism (Lipman *et al.*, 1978; Riciputi *et al.*, 1995), the composition of the basaltic parental magmas remains unknown and the nature of the mantle source(s) for this vast outpouring of intermediate to silicic magmas remains poorly constrained.

Table 2: Representative whole-rock major and trace element and radiogenic isotope data for samples of the Huerto Andesite

	Trachyandesitic lavas										
	Ribbon Mesa				Sugarloaf Mountain				Baldy Mountain		
Sample:	HA25	HA27[1]	HA28[1]	HA29[1]	HA30	HA31[1]	HA32	HA33[1]	HA34	HA35[2]	HA37[1]
wt %											
SiO_2	57·66	56·94	59·24	59·14	58·13	61·19	55·65	58·19	56·22	55·78	55·85
TiO_2	1·07	1·07	1·00	1·00	1·31	1·17	1·06	1·28	1·10	1·12	1·05
Al_2O_3	18·30	17·86	18·05	17·65	16·38	17·22	18·12	16·57	17·10	17·48	18·60
Fe_2O_3*	6·52	6·90	5·60	6·09	8·06	6·32	8·57	8·01	9·17	9·33	8·33
MnO	0·10	0·15	0·12	0·19	0·12	0·01	0·14	0·18	0·15	0·14	0·14
MgO	2·52	2·27	1·78	1·90	2·07	1·23	2·56	2·33	3·26	3·15	2·40
CaO	6·08	7·10	6·50	6·43	5·75	4·43	6·66	5·32	6·70	6·64	6·67
Na_2O	4·02	3·99	3·58	3·50	3·57	4·18	3·83	3·65	3·73	3·77	4·19
K_2O	3·15	3·14	3·70	3·67	3·88	3·65	2·86	3·73	2·17	2·18	2·24
P_2O_5	0·57	0·57	0·42	0·42	0·73	0·61	0·55	0·72	0·40	0·42	0·52
Original total	99·19	98·58	99·29	99·20	98·58	98·68	99·08	99·69	100·20	99·22	99·02
ppm											
Ba	880	867	926	856	870	910	867	936	855	845	879
Rb	68	66	92	96	113	107	65	112	48	40	33
Sr	684	681	602	582	504	463	697	495	662	663	739
Ta										0·65	
Th	4	<2	11	12	7	11	3	13	8	5	5
Zr	209	213	304	302	405	388	222	400	169	202	212
Nb	12	13	16	16	24	23	13	25	7	11	11
Y	36	34	34	34	47	36	32	47	31	28	33
Hf	5	4	8	5	10	7	6	6	7	5	3
V	110	108	119	119	114	97	135	118	179	171	114
Cr	5	5	10	10	6	<2	5	2	31	18	<2
Ni	<2	<2	9	10	6	<2	7	3	10	13	<2
Co	21	16	13	16	19	17	27	17	29	23	17
Cu	19	16	59	51	27	24	20	31	39	34	22
Zn	86	87	85	85	103	113	93	114	104	105	108
La	37	34·0	38·4	48·0	48	40·0	34	50·5	29	27·4	29·4
Ce	104	80·0	83·0	101·0	129	118·0	94	113·1	61	58·4	63·2
Pr		9·5	9·7	9·9				13·2		7·3	8·0
Nd	50	39·0	42·0	53·0	58	54·0	46	59·5	36	32·3	36·5
Sm		8·2	8·6	9·0		8·0		12·2		6·6	7·7
Eu		1·91	1·92	1·93		1·91		2·51		1·83	2·22
Gd		6·6	6·4	7·0		6·5		9·1		5·2	6·5
Tb										0·8	
Dy		5·9	5·8	6·1		6·0		8·4		5·2	6·3
Ho		1·1	1·1	1·1		1·0		1·8		1·1	1·3
Er		2·8	2·9	3·0		2·9		4·4		2·7	3·3
Tm		0·4	0·4	0·4		0·4		0·6		0·4	0·5
Yb		2·6	2·6	2·7		2·7		3·9		2·1	2·9
Lu		0·39	0·38	0·40		0·39		0·48		0·30	0·43

Table 2: Continued

	Trachyandesitic lavas										
	Ribbon Mesa				Sugarloaf Mountain				Baldy Mountain		
Sample:	HA25	HA27[1]	HA28[1]	HA29[1]	HA30	HA31[1]	HA32	HA33[1]	HA34	HA35[2]	HA37[1]
Pb	13	15	15	16	20	16	15	18	19	8	8
S	<3	37	36	51	<3	<3	<3	<3	<3	<3	<3
$^{87}Sr/^{86}Sr$		0·705906	0·705500	0·705496		0·705632		0·705848		0·705951	
$^{87}Sr/^{86}Sr_{(i)}$		0·705791	0·705324	0·705307		0·705367		0·705587		0·705882	
$^{143}Nd/^{144}Nd$		0·512275	0·512264	0·512272		0·512255		0·512308		0·512314	
$^{143}Nd/^{144}Nd_{(i)}$		0·512252	0·512241	0·512254		0·512239		0·512285		0·512291	
$^{206}Pb/^{204}Pb$		18·669	18·611	18·615		18·630		18·581		18·357	
$^{207}Pb/^{204}Pb$		15·581	15·577	15·578		15·584		15·580		15·561	
$^{208}Pb/^{204}Pb$		37·953	37·921	37·951		37·871		37·945		37·832	

	Trachyandesitic lavas		Calc-alkaline lavas							
	Baldy Mountain		West Fork San Juan River							
Sample:	HA38	HA39[1]	HA6[1]	HA9	HA10[1]	HA12	HA14[1]	HA16	HA17[1]	HA18[1]
wt %										
SiO_2	56·02	58·53	59·78	58·16	61·83	60·47	57·80	61·49	64·56	62·20
TiO_2	1·10	1·17	0·70	0·86	0·66	0·72	0·88	0·66	0·69	0·65
Al_2O_3	17·63	17·15	18·00	17·56	17·12	18·15	17·78	16·94	17·06	18·11
Fe_2O_3*	9·02	7·80	6·20	7·40	5·79	5·62	7·56	5·98	5·20	4·74
MnO	0·15	0·09	0·16	0·17	0·14	0·15	0·16	0·12	0·07	0·09
MgO	3·01	1·86	2·35	3·08	2·19	2·23	2·99	2·74	0·66	1·65
CaO	6·54	5·47	6·24	6·60	5·67	6·07	6·58	5·65	5·00	5·58
Na_2O	3·87	3·85	3·65	3·38	3·95	3·24	3·37	3·81	3·69	4·08
K_2O	2·23	3·45	2·51	2·47	2·38	2·95	2·50	2·36	2·79	2·51
P_2O_5	0·43	0·62	0·40	0·32	0·27	0·41	0·37	0·25	0·27	0·39
Original total	99·12	98·92	99·02	99·22	99·26	98·55	98·90	98·79	99·63	99·94
ppm										
Ba	865	987	776	860	828	829	877	818	866	859
Rb	38	81	42	45	43	53	38	47	48	43
Sr	704	578	765	698	785	744	737	785	721	725
Ta										
Th	<2	4	5	<2	<2	<2	5	<2	<2	6
Zr	177	251	197	171	128	205	198	120	136	212
Nb	10	15	9	7	5	8	9	6	6	9
Y	30	37	25	27	21	29	26	19	20	32
Hf	4	6	3	3	4	6	4	5	4	4
V	159	101	76	152	109	72	133	119	97	65
Cr	14	5	2	15	14	3	6	23	18	<2
Ni	11	<2	5	8	7	<2	3	9	4	<2
Co	22	14	14	22	12	11	20	15	9	12
Cu	29	25	13	24	18	13	20	22	21	11
Zn	95	102	94	88	76	94	95	78	54	135

	Trachyandesitic lavas		Calc-alkaline lavas							
	Baldy Mountain		West Fork San Juan River							
Sample:	HA38	HA39[1]	HA6[1]	HA9	HA10[1]	HA12	HA14[1]	HA16	HA17[1]	HA18[1]
La	24	39·0	41	29	28·3	34	28·0	21	20·6	32·3
Ce	68	102·0	58	63	57·4	69	59·4	43	40·3	72·0
Pr		9·6			7·2		6·9		5·0	8·6
Nd	32	47·0	36	32	28·4	34	29·9	21	19·6	37·8
Sm		8·8	6·1		5·7		6·6		3·9	7·7
Eu		1·82	1·7		1·75		1·67		1·21	1·9
Gd		5·5	5·3		6·0		4·8		3·9	5·8
Tb					0·7				0·5	
Dy		5·4	4·2		4·1		4·6		2·7	5·6
Ho		1·2	0·9		0·8		0·97		0·54	1·21
Er		3·1	2·3		2·3		2·5		1·5	3·2
Tm		0·4	0·4				0·37			0·48
Yb		2·5	2·28		2·2		2·3		1·4	3·1
Lu		0·42	0·34		0·33		0·34		0·2	0·47
Pb	13	21	9	13	14·2	15	10	17	8·4	11
S	<3	<3	260	5	<3	<3	<3	<3	<3	143
$^{87}Sr/^{86}Sr$			0·704981				0·705065			0·705212
$^{87}Sr/^{86}Sr_{(i)}$			0·704918				0·705006			0·705143
$^{143}Nd/^{144}Nd$		0·512243	0·512150				0·512120			0·512203
$^{143}Nd/1^{44}Nd_{(i)}$		0·512229	0·512047				0·512096			0·512180
$^{206}Pb/^{204}Pb$			18·098				17·912			18·139
$^{207}Pb/^{204}Pb$			15·532				15·509			15·545
$^{208}Pb/^{204}Pb$			37·538				37·459			37·602

	Calc-alkaline lavas				Calc-alkaline dykes							
	West Fork San Juan River				Eagle Mountain			Fourmile Creek				
Sample:	HA19	HA20	HA22[1]	HA23	EMA13[2]	EMA4[1]	EMA9[1]	DA10[1]	DA4[1]	HA1[1]	HA2	HA4
wt %												
SiO_2	61·58	57·68	62·19	58·93	62·90	62·38	63·32	63·22	62·09	63·93	64·17	62·98
TiO_2	0·60	0·86	0·63	0·77	0·71	0·73	0·71	0·72	0·75	0·63	0·62	0·72
Al_2O_3	17·76	17·48	17·24	18·04	16·94	17·01	16·93	17·01	16·85	17·20	17·07	17·27
Fe_2O_3*	5·72	8·18	5·59	6·99	5·50	5·62	5·26	5·53	5·96	5·11	5·08	5·08
MnO	0·16	0·12	0·14	0·16	0·07	0·08	0·07	0·08	0·08	0·06	0·06	0·10
MgO	2·02	2·87	2·26	2·73	1·84	1·85	1·56	1·75	2·01	1·45	1·55	1·79
CaO	5·63	6·69	5·80	6·39	5·10	5·36	5·12	4·54	5·35	4·72	4·68	4·96
Na_2O	3·84	3·59	3·32	3·32	4·08	4·08	4·15	3·94	4·02	4·06	4·01	3·94
K_2O	2·37	2·13	2·57	2·34	2·54	2·56	2·57	2·89	2·55	2·57	2·49	2·82
P_2O_5	0·31	0·40	0·26	0·33	0·32	0·33	0·32	0·32	0·34	0·26	0·26	0·33
Original total	99·57	99·07	98·94	98·61	98·17	99·55	100·05	99·30	99·86	99·48	99·34	98·24
ppm												
Ba	801	773	804	802	681	911	904	961	864	842	821	800
Rb	50	35	50	41	36	55	53	65	46	41	41	54

Table 2: Continued

	Calc-alkaline lavas				Calc-alkaline dykes							
	West Fork San Juan River				Eagle Mountain				Fourmile Creek			
Sample:	HA19	HA20	HA22[1]	HA23	EMA13[2]	EMA4[1]	EMA9[1]	DA10[1]	DA4[1]	HA1[1]	HA2	HA4
Sr	673	862	729	725	708	888	909	796	851	781	762	770
Ta					0·46							
Th	12	<2	8	<2	3	<2	5	8	5	4	5	<2
Zr	140	148	136	172	122	136	131	131	170	159	164	137
Nb	5	7	3	8	8	3	3	4	9	8	8	8
Y	28	26	27	25	13	19	17	16	14	11	11	15
Hf	7	4	6	5	3	6	6	6	7	4	6	5
V	66	116	86	108	72	88	80	71	86	59	58	72
Cr	21	3	13	25	7	9	17	10	24	5	4	11
Ni	<2	4	<2	2	2	3	<2	<2	2	<2	<2	6
Co	13	19	14	17	12	52	17	13	14	11	10	14
Cu	18	14	18	19	22	21	23	21	24	14	21	20
Zn	86	88	79	82	41	79	84	77	80	69	80	80
La	42	22	23·6	33	23·8	23·8	25·2	22·9	22·9	21·6	26	20
Ce	61	52	46·6	57	50·3	52·7	54·7	51·2	51·2	46·0	45	54
Pr			5·7		6·4	6·3	6·2	5·4	5·4	5·5		
Nd	35	23	26·5	28	25·3	26·8	28·1	25·1	25·1	23·1	23	24
Sm			4·90		4·95	5·90	6·10	5·50	5·50	4·50		
Eu			1·42		1·52	1·53	1·59	1·51	1·51	1·33		
Gd			3·90		4·69	3·20	4·10	3·70	3·70	3·50		
Tb					0·57							
Dy			4·00		2·49	2·90	2·80	2·60	2·60	2·30		
Ho			0·83		0·43	0·53	0·51	0·44	0·44	0·45		
Er			2·30		1·02	1·10	1·10	1·00	1·00	0·90		
Tm			0·35		—	0·13	0·15	0·14	0·14	0·13		
Yb			2·10		0·85	0·80	0·90	0·90	0·90	0·70		
Lu			0·30		0·13	0·12	0·14	0·13	0·13	0·09		
Pb	20	17	21	15	12	25	24	22	10	11	12	17
S	9	<3	19	<3	<3	51	43	153	189	6	26	<3
$^{87}Sr/^{86}Sr$					0·704537		0·704421	0·704506		0·704476		
$^{87}Sr/^{86}Sr_{(i)}$					0·704456		0·704327	0·704439		0·704416		
$^{143}Nd/^{144}Nd$					0·512176			0·512176				
$^{143}Nd/^{144}Nd_{(i)}$					0·512154			0·512152				
$^{206}Pb/^{204}Pb$							18·092	18·105		18·056		
$^{207}Pb/^{204}Pb$							15·543	15·547		15·523		
$^{208}Pb/^{204}Pb$							37·364	37·353		37·301		

Major and trace elements obtained by X-ray fluorescence (XRF) spectrometry [University of Lausanne, method of Rhodes (1988)]. Major elements are normalized to 100% on a volatile-free basis. Sr–Nd and Pb isotopic compositions were determined at the University of Geneva using the method of Schilling *et al*. (1994) and Chiaradia & Fontboté (2003), respectively. Subscript (i) indicates isotopic ratio corrected at 28 Ma.

[1]Rare earth elements (REE) obtained by inductively coupled plasma atomic emission spectroscopy [ICP-AES, University of Geneva, method of Voldet (1993)].

[2]REE obtained by inductively coupled plasma mass spectrometry (ICP-MS) (REE + Ta) [University of Grenoble, method of Barrat *et al*. (1996)].

For the Huerto Andesite, were there two distinct parental magma sources for the trachyandesite and calc-alkaline series, or do these two lineages represent contrasting evolution paths from a single parental magma as a result of differentiation under contrasting conditions? Having established the differences between the two series, we address this question on the basis of major and trace element and isotopic compositions of Huerto lavas and dykes.

Major and trace element chemistry

Differences in mineralogy and mineral chemistry between the trachyandesitic and calc-alkaline series are manifestations of their generally distinct major element trends (Fig. 2) in combination with differences in oxygen fugacity (Fig. 9). In addition to its higher alkali–lime index, higher total alkalis and less marked suppression of Fe enrichment relative to a tholeiitic trend (Grove & Kinzler, 1986), the trachyandesitic series is distinguished by greater depletions of CaO, MgO and Al_2O_3 and constant or increasing P_2O_5, K_2O and TiO_2 with respect to increasing SiO_2 than the calc-alkaline series (Fig. 10, Table 2).

In comparison, fields for magma compositions from the Horseshoe Mountain member (hornblende-bearing calc-alkaline andesitic series) and Rock Creek member (anhydrous mineralogy, mildly alkaline series) of the Conejos Formation (Colucci *et al.*, 1991), which are similar to the Huerto calc-alkaline and trachyandesitic series, respectively, display similar compositional distinctions, particularly for P_2O_5, K_2O, TiO_2, Rb, Zr, Nb, rare earth elements (REE) and Y (Figs 10 and 11). These parallels between Conejos and Huerto volcanism suggest that the processes and/or conditions responsible for the development of divergent differentiation trends during restricted time intervals occurred repeatedly during San Juan volcanism.

The most mafic samples of each series (basaltic trachyandesite, mafic calc-alkaline andesite) have similar major element contents (particularly for K_2O, total alkalis and P_2O_5), trace element contents and trace element ratios: the most mafic trachyandesitic lavas (55–56 wt % SiO_2) have slightly lower concentrations for some incompatible elements than do the most mafic calc-alkaline andesites (57 wt % SiO_2). With differentiation, the two trends diverge. In the trachyandesite range, the mildly alkaline lavas have systematically higher incompatible element contents for a given SiO_2, up to two times higher (e.g. K_2O, TiO_2, Rb, Ce, Y, Nb, Zr) and lower compatible element concentrations (e.g. FeO, MgO, CaO, Al_2O_3 and Sr), than the calc-alkaline series (Figs 10 and 11). Basaltic trachyandesites are characterized by large ranges in incompatible elements over a narrow range in SiO_2 (e.g. 190–405 ppm Zr, 10–24 ppm Nb, 28–47 ppm Y, 30–115 ppm Rb). Sr content decreases from 700 to nearly 400 ppm in the trachyandesite series and the most evolved magmas are characterized by small negative Eu anomalies (Fig. 12c). Rb and Sr both increase with increasing SiO_2 in the calc-alkaline series, whereas elements such as the light rare earth elements (LREE) and high field strength elements (HFSE) remain constant or decrease slightly, and the heavy REE (HREE) and Y show significant decreases.

All mafic and evolved lavas, regardless of location or series, are depleted in HFSE relative to large ion lithophile elements (LILE) and LREE (e.g. Rb/Zr = 0·2–0·5; Ba/Nb = 40–100 [0·01 and 2·7 in mid-ocean ridge basalt (MORB) respectively; Sun & McDonough, 1989; Fig. 12a and b] and they are enriched in LREE relative to HREE (Fig. 12c and d). Andesites from the WFSJR have both lower and higher incompatible element contents than associated mafic andesites and, therefore, also define two divergent trends for certain elements (e.g. LREE, Y and HREE). The Fourmile Creek andesites are similar to the WFSJR andesites that have relatively low Y, Zr, Nb and HREE (Figs 11 and 12).

Sr, Nd and Pb isotope compositions

Sr–Nd–Pb isotope ratios determined for 12 Huerto samples generally fall within the ranges determined by Riciputi *et al.* (1995) in a survey of central San Juan tuffs and lavas (Table 2, Fig. 13). Although we have drawn some analogies between the Huerto calc-calkaline lavas and the hornblende-bearing Horseshoe Mountain member of the Conejos Formation in the SE San Juan volcanic field, the relatively non-radiogenic Pb isotopic compositions of the Horseshoe Mountain lavas are not matched by any Huerto lavas. We note, however, that the offset of the trachyandesitic Huerto lavas toward higher $^{206}Pb/^{204}Pb$ and $^{208}Pb/^{204}Pb$ relative to Huerto calc-alkaline lavas is analogous to Pb-isotope differences between Horsehoe Mountain and Rock Creek member lavas of the Conejos Formation (Colucci *et al.*, 1991; Fig. 13a). The sampled Horseshoe Mountain member is located exclusively around the eastern and northeastern margins of the Platoro caldera and it is far less radiogenic in Pb than lavas of broadly similar composition located around the western margin of the Platoro caldera (M. A. Dungan & S. Moorbath, unpublished data) or anywhere in the central San Juan volcanic field. These observations suggest that local and regional differences in isotopic character of the crust on which the San Juan volcanic field is constructed are significant.

Trachyandesitic lavas have higher Nd, Pb and Sr isotope ratios than the calc-alkaline lavas. These differences are most pronounced between the most mafic lavas of the two series, particularly for $^{143}Nd/^{144}Nd$. Thus, if

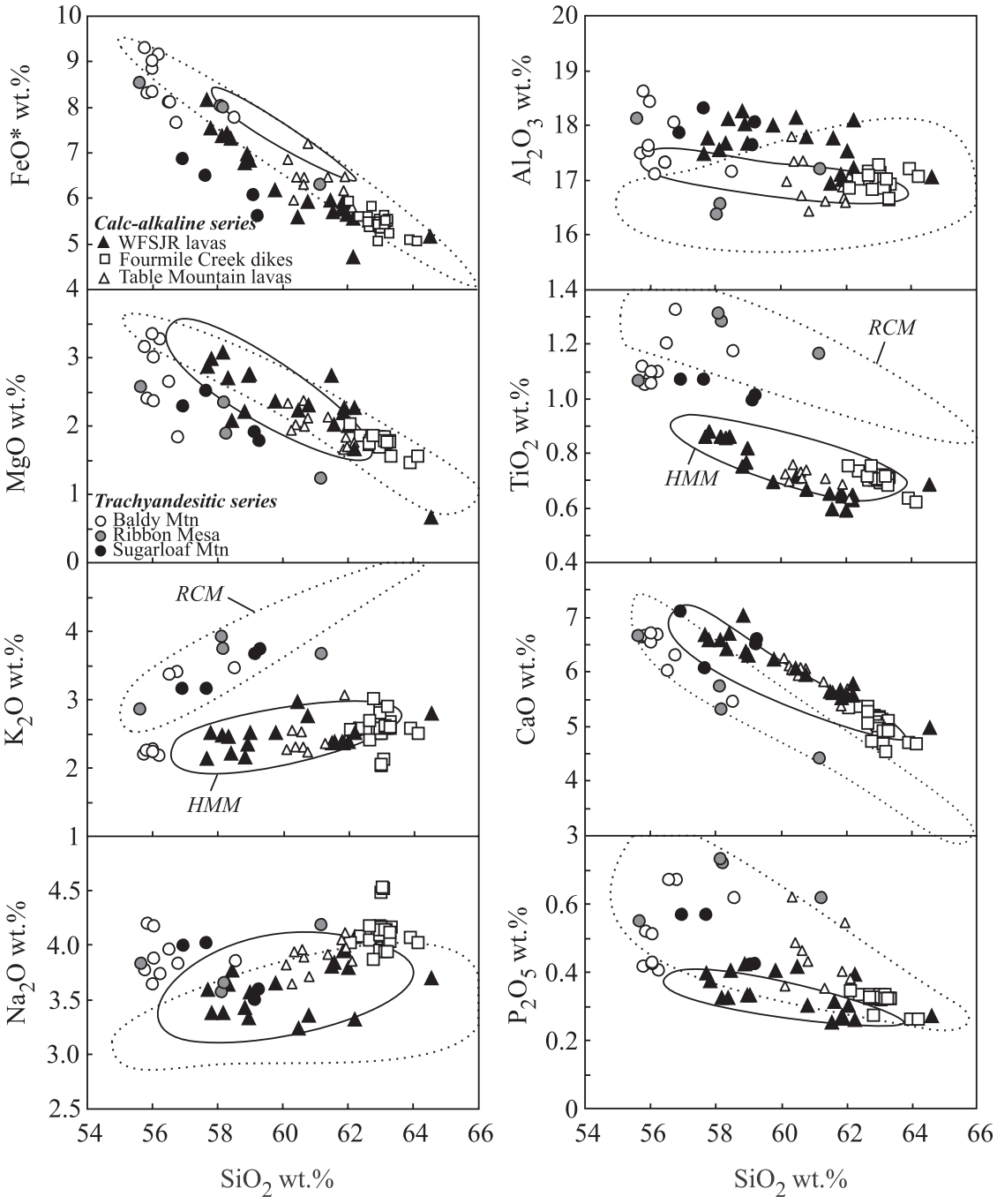

Fig. 10. Major element (anhydrous) variation diagrams plotted against wt % SiO_2 (anhydrous) for lavas and dykes of the Huerto Andesite. Fields labelled RCM and HMM are for Rock Creek and Horseshoe Mountain members of the Conejos Formation (Colucci *et al.*, 1991). WFSJR, West Fork of the San Juan River. Data for Table Mountain lavas from Christie (2001).

parental basaltic magmas for the two series were similar, the contrasting cryptic phases of differentiation leading to the least evolved sampled magmas of the two series were characterized by assimilation of very different crustal lithologies. The trachyandesitic lavas define weak trends of decreasing $^{87}Sr/^{86}Sr_{(i)}$ and $^{144}Nd/^{143}Nd_{(i)}$ with increasing SiO_2, but Pb isotopes vary less systematically (Fig. 14). The relatively narrow ranges of isotopic variations in trachyandesitic series lavas from the three volcanic centres that are widely dispersed around the periphery of the La Garita caldera are in accord with the absence of systematic differences in mineralogy, as

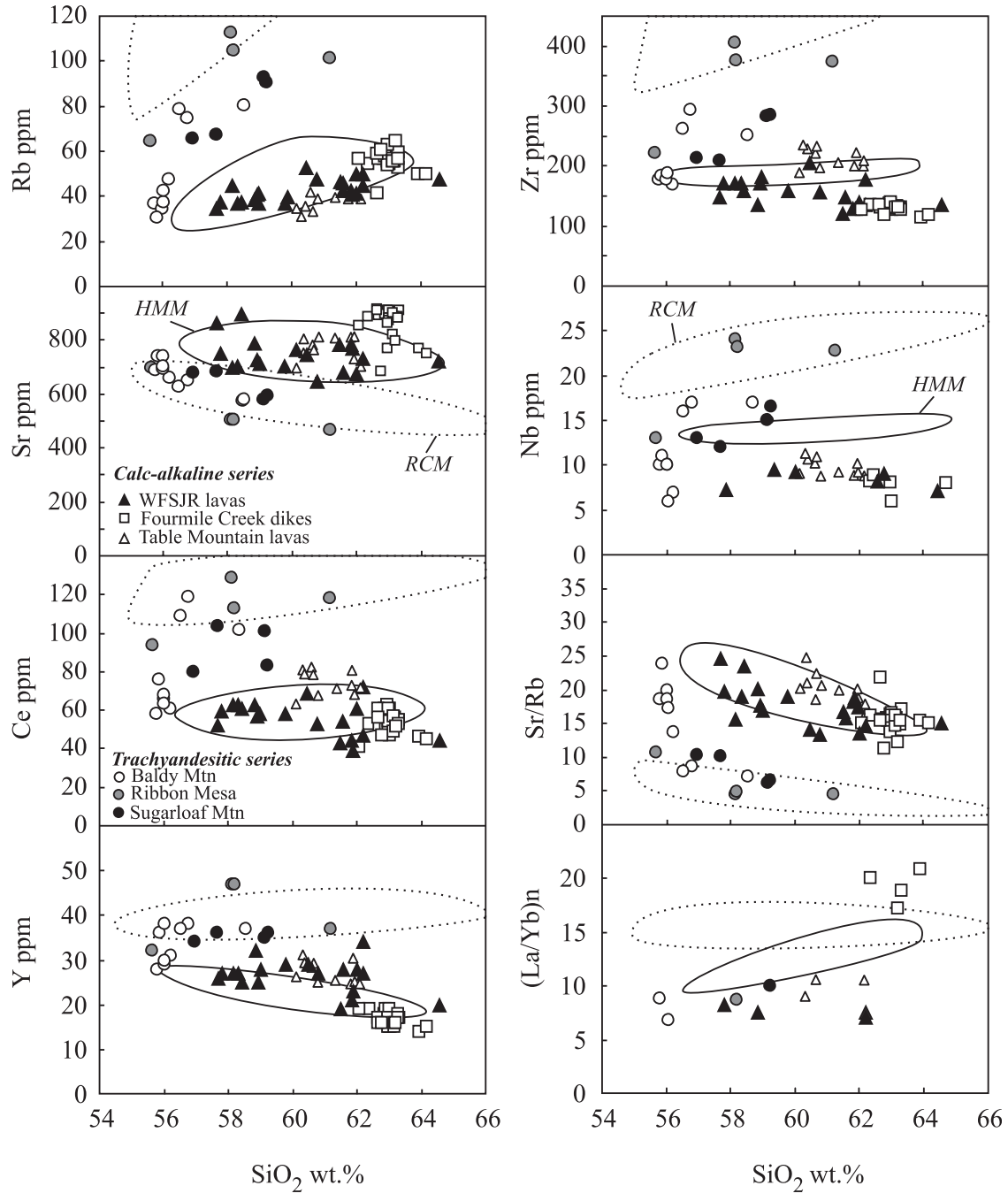

Fig. 11. Trace element variation diagrams plotted against wt % SiO_2 (anhydrous) for lavas and dykes of the Huerto Andesite. $(La/Yb)_n$ normalized using the chondrite values of Boynton (1984). Fields labelled RCM and HMM are for Rock Creek and Horseshoe Mountain members of the Conejos Formation (Colucci *et al.*, 1991). WFSJR, West Fork of the San Juan River. Data for Table Mountain lavas from Christie (2001).

well as the major and trace element compositions. In contrast, samples from the adjacent Fourmile Creek and WFSJR calc-alkaline centres define separate isotopic populations that correspond to the two groups that were defined above on the basis of HREE and Y concentrations.

PETROGENESIS OF HUERTO ANDESITE MAGMAS

In this section, multiple models that address compositional diversity among Huerto magmas are evaluated using the available geochemical and isotopic data

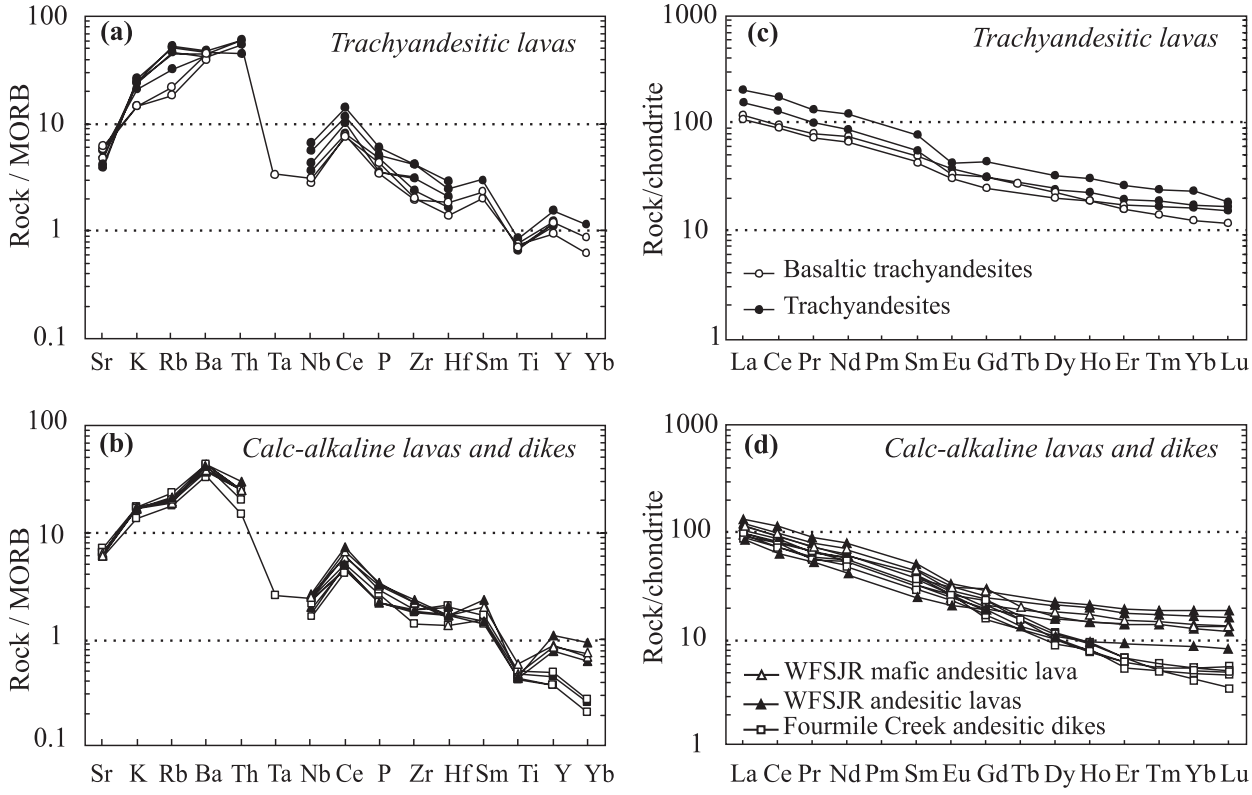

Fig. 12. (a, b) MORB-normalized trace element variation diagrams and (c, d) chondrite-normalized REE diagrams for the Huerto Andesite. Data normalized using the MORB values of Sun & McDonough (1989) and the chondrite values of Boynton (1984). WFSJR, West Fork of the San Juan River.

(Table 2). The approximate proportions of phenocryst phases that could have been involved during fractionation from mafic to more evolved magmas have been estimated by least-squares regression analysis using observed phase compositions. We acknowledge that none of these evolved magmas is a pure product of fractionation and therefore do not imply that these estimates are quantitatively correct. As fractional crystallization alone is inadequate to account for variations in incompatible elements and the ranges of isotopic ratios, open-system processes are required and multiple parental magma compositions were probably involved in both series. Calculated mineral proportions are used as input for trace element models involving both magma mixing and fractional crystallization coupled with crustal assimilation. The least evolved magma in each series was selected as the putative parental composition for evaluating progressive differentiation (HA37 for trachyandesites, HA14 for WFSJR calc-alkaline lavas). As little direct evidence constrains the compositions of crustal lithologies beneath the San Juan volcanic field, we use a range of plausible components for illustrative purposes.

Differentiation of the trachyandesitic magma series

There are no systematic geographical differences in mineralogy, and only limited distinctions in terms of geochemistry (Baldy Mountain lavas tend to be less incompatible element-enriched than lavas from Ribbon Mesa or Sugarloaf Mountain), among the three centres. Trachyandesitic lavas are variably but strongly enriched in incompatible elements and only moderately depleted in compatible trace elements over a restricted range of intermediate major element compositions (~55–62 wt % SiO_2). These patterns define broad fields rather than linear trends, indicating that no single model can account for all the variations. This combination of observations, particularly the rapid elevations of incompatible element concentrations without dramatic depletions of compatible elements, requires open-system processes in addition to fractional crystallization. Least-squares regression using the composition of the mafic sample HA37 and the compositions of phenocryst phases in trachyandesitic lavas (HA31; Table 3) leads to a reasonable approximation of an evolved trachyandesite (TiO_2

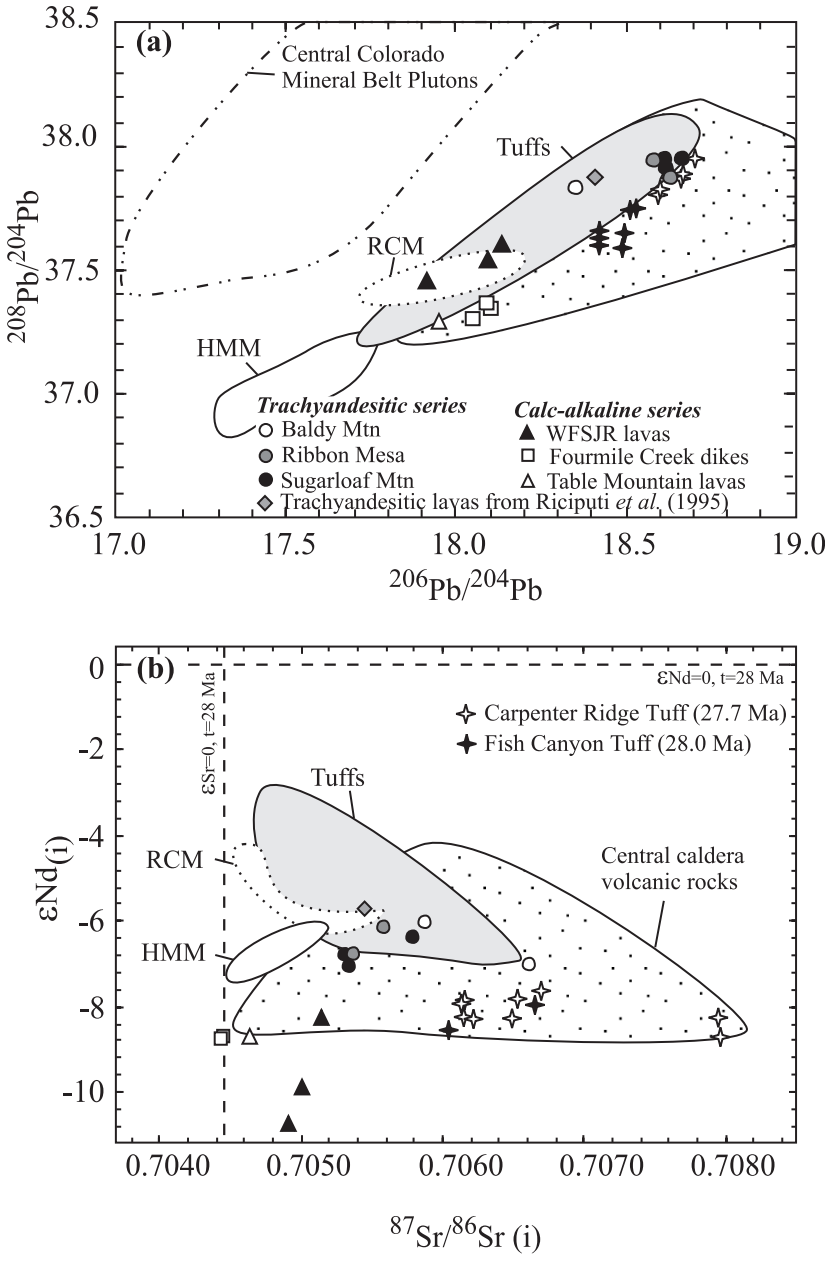

Fig. 13. (a) $^{208}Pb/^{204}Pb$ vs $^{206}Pb/^{204}Pb$ and (b) εNdi vs $^{87}Sr/^{86}Sr_{(i)}$ for whole-rock samples of the Huerto Andesite and associated volcanic rocks. WFSJR, West Fork of the San Juan River. Conejos Formation (Colucci *et al.*, 1991): HMM, Horseshoe Mountain; RCM, Rock Creek Mountain. Fish Canyon Tuff and Carpenter Ridge Tuff data from Riciputi *et al.* (1995). Central caldera rocks from Riciputi *et al.* (1995) and Central Colorado Mineral Belt Plutons from Stein (1985).

and K_2O are too low, FeO and CaO are too high in the calculated daughter) and the calculated phase proportions are in fair agreement with the observed phenocryst assemblage. The abundance of plagioclase (>50% of total phenocrysts) is in accord with the trend of decreasing Sr with increasing SiO_2. From this we conclude that fractional crystallization played a role in generating this spectrum of magmas. None the less, the calculated decrease in Sr for fractionation of this plagioclase-rich assemblage is less than one-third of the observed decrease and other anomalies are observed. One of these is the limited enrichment of Ba (<twofold; Fig. 12a) compared with those observed for comparably incompatible elements during fractionation of an anhydrous mineral assemblage; i.e., Rb, K, Zr, Th and Nb exhibit well-correlated threefold to fourfold enrichments (post-emplacement alteration of these glassy lavas is not a factor) and LREE increase by a factor of

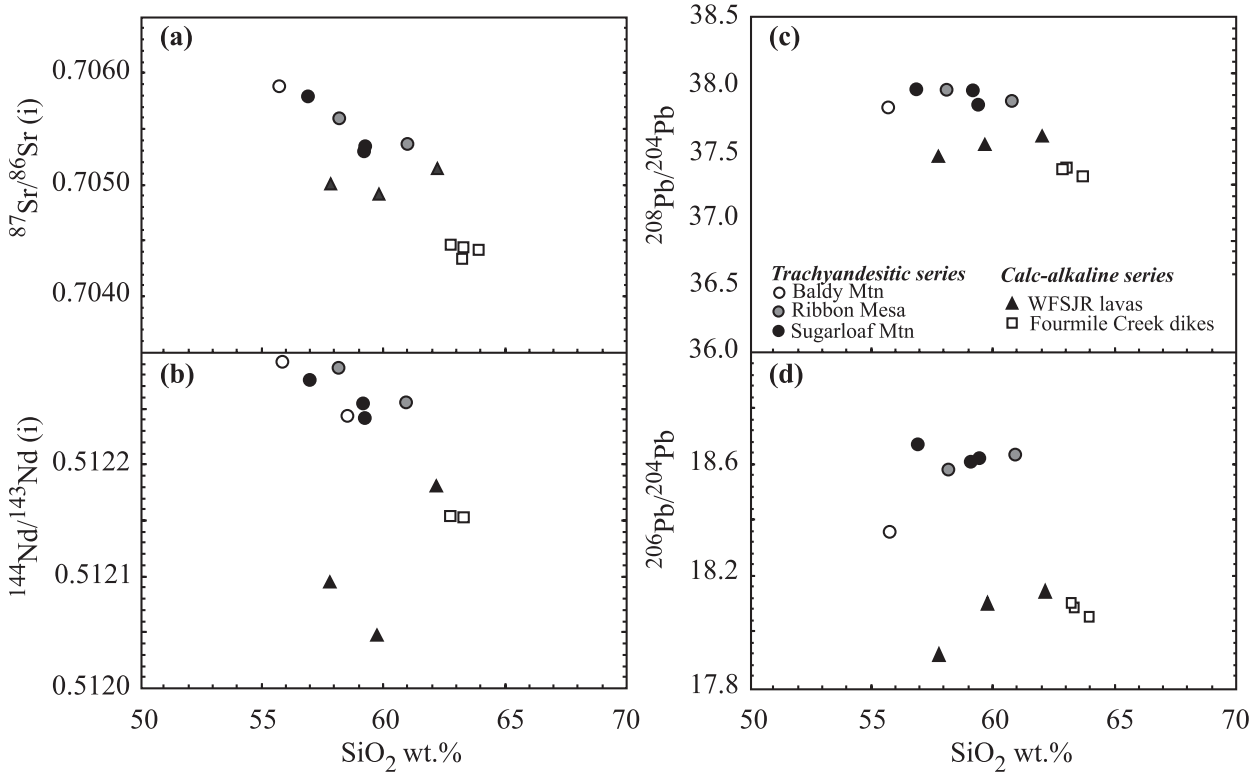

Fig. 14. (a) Sr, (b) Nd, and (c, d) Pb isotopic compositions vs wt % SiO_2 concentrations (anhydrous) for whole-rock samples of the Huerto Andesite. WFSJR, West Fork of the San Juan River.

Table 3: Major element fractional crystallization models for Huerto Andesite

	Trachyandesitic magmas						Calc-alkaline magmas					
	Parent	Daughter	Calc. daughter	Residual	Subtracted phases	Vol. %	Parent	Daughter	Calc. daughter	Residual	Subtracted phases	Vol. %
Sample:	HA37	HA31					HA14	HA18				
wt % (anhydrous)												
SiO_2	55·85	60·97	60·80	0·09	Plag	24·1	57·68	61·84	61·82	−0·01	Plag	7·8
TiO_2	1·05	1·16	0·91	0·25	Ol	2·3	0·86	0·65	0·55	0·10	Amph	4·0
Al_2O_3	18·60	17·16	17·13	−0·05	Cpx	6·4	17·48	18·00	18·00	0·00	Cpx	2·2
FeO*	8·33	6·30	7·21	−0·16	Opx	2·7	8·18	5·30	5·31	−0·01	Opx	2·7
MnO	0·14	0·10	0·08	−0·07	Mag	4·7	0·12	0·09	0·07	0·02	Mag	3·1
MgO	2·40	1·22	1·19	0·03	Apa	0	2·87	1·64	1·65	−0·01	Apa	0·2
CaO	6·67	4·42	4·53	−0·13	Dght%	40·2	6·69	5·55	5·56	−0·01	Dght%	20·0
Na_2O	4·19	4·10	4·11	0·04			3·59	4·05	4·07	−0·02		
K_2O	2·24	3·95	3·36	0·27	Σr^2	0·20	2·13	2·49	2·61	−0·12	Σr^2	0·025
P_2O_5	0·52	0·62	0·68	−0·08			0·40	0·39	0·37	0·02		

Compositions normalized to 100% anhydrous. Σr^2, sum of the square of the residuals.

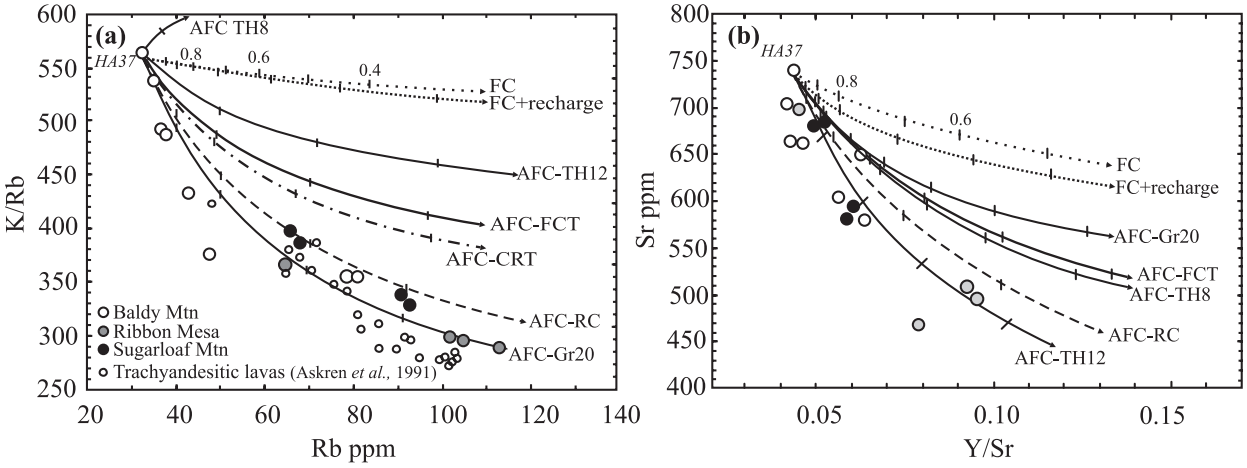

Fig. 15. (a) K/Rb vs Rb and (b) Sr vs Y/Sr plots for trachyandesitic lavas. Model curves represent closed-system crystallization (FC), combined assimilation–fractional crystallization (AFC) and combined recharge–fractional crystallization from the more mafic sample (HA37) calculated after the method of DePaolo (1981). Partition coefficients used in the modelling are from Rollinson (1993). The AFC curves depict assimilation of Carpenter Ridge Tuff [CRT: LZ49 of Whitney *et al.* (1988)], Fish Canyon Tuff [FCT: FCTpum(I) of Bachmann *et al.* (2000)], Rock Creek lavas [RC: CoV-200 of Colucci *et al.* (1991)] and A-type granite (TH12, TH8 and Gr20; Latysh, 1997; Condie *et al.*, 1999) at a mass assimilation rate/crystallization rate (r) of 0·5. Tick marks on curves represent the percentage of magma remaining after crystallization (10% increments).

two from mafic trachyandesite to trachyandesite. Also, very low Cr values (~5–10 ppm) clearly indicate that trachyandesites are strongly fractionated magmas, but SiO_2 values around 56 wt % for the most enriched samples require some process to keep them at this mafic silica value. Recharge offsets the depletion in Cr and prevents the silica enrichment that would occur if fractionation and assimilation of silicic contaminant were the main means of incompatible element enrichment.

The temporal and spatial association of the Huerto Andesite with the La Garita caldera offers the possibility that interaction of mafic Huerto magmas with silicic magmas residing in the crust may have occurred. The dacitic Fish Canyon Tuff and the rhyolitic Carpenter Ridge Tuff, which stratigraphically bracket the Huerto Andesite, are potential candidates for such interactions. Even though these tuffs collectively range from dacite to rhyolite they have lower concentrations of many incompatible trace element than do Huerto trachyandesitic lavas (e.g. <300 ppm Zr; <180 Ce ppm; Dorais *et al.*, 1991; Bachmann *et al.*, 2000). If these compositions are representative of local silicic magmas, evolved trachyandesitic magmas with 200–400 ppm Zr and K/Rb >250 cannot result from magma mixing with these or similar magmas nor from fractional crystallization + magma mixing (AFC, Fig. 15). The high $^{87}Sr/^{86}Sr_{(i)}$ (0·70605–0·70797; Fig. 13) and moderately high Sr concentrations of these tuffs also raise the $^{87}Sr/^{86}Sr$ in calculated evolved compositions to values well beyond the observed $^{87}Sr/^{86}Sr_{(i)}$ of trachyandesitic magmas (AFC model, Fig. 16).

Among the potential crustal compositions, which have the elevated incompatible trace element concentrations and low Ba concentration required by the differentiated trachyandesitic Huerto magmas, are A-type granitoids typical of those that were widespread in the southern Rocky Mountain region in the Proterozoic (e.g. Silver & McGetchin, 1994; Condie *et al.*, 1999). AFC models utilizing Rb-rich compositions from these granites (Gr20 and Th12; Fig. 15) provide good matches for most incompatible-element enrichments in the trachyandesitic suite and for changes in some elemental ratios. However, Rb-rich Proterozoic samples cannot have low $^{87}Sr/^{86}Sr$ ratios to provide the range of $^{87}Sr/^{86}Sr$ of the trachyandesitic lavas (Fig. 16), as granitoid xenoliths with low $^{87}Sr/^{86}Sr$ have low Rb concentration [e.g. $^{87}Sr/^{86}Sr$ ratios range from 0·70442 (GR-1: Rb 39·6 ppm) to 0·73825 (Th12: Rb 127·5 ppm) in granitoid xenoliths from Navajo Volcanic Field; Condie *et al.*, 1999; Figs 15 and 16]. The crustal contributions were probably supplied by partial melting or assimilation of evolved but slightly older subvolcanic plutons (e.g. Conejos rocks, Figs 15 and 16) that could provide the same combination of high incompatible element enrichments and low $^{87}Sr/^{86}Sr$ that is required by the Huerto data.

Differentiation of calc-alkaline magma series

With regard to the calc-alkaline magma series, the geographical differences in geochemistry and, to a lesser extent, in mineralogy among the WFSJR lavas and Fourmile Creek dykes of the calc-alkaline series require

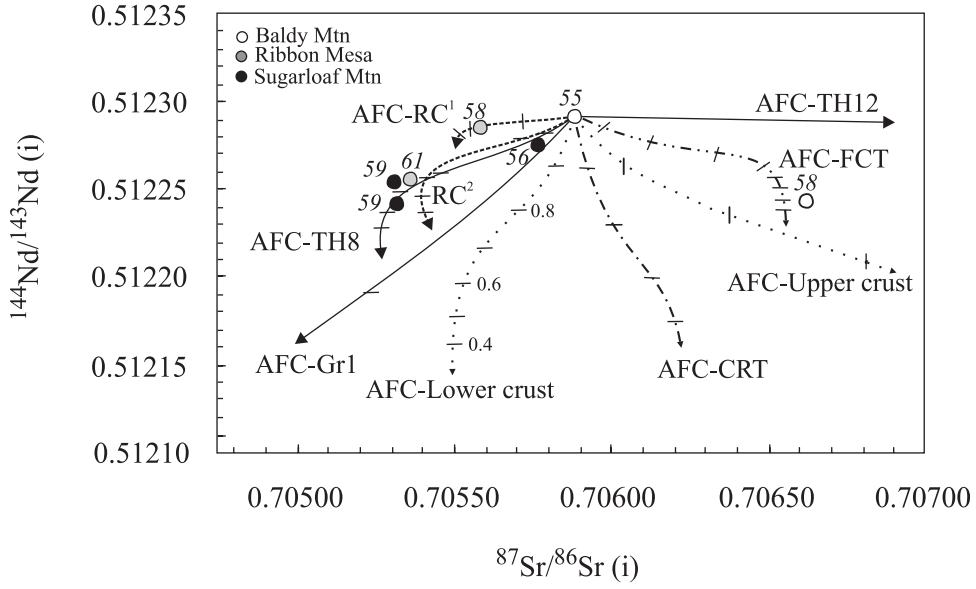

Fig. 16. Calculated assimilation–fractional crystallization models for $^{87}Sr/^{86}Sr_{(i)}$ vs $^{144}Nd/^{143}Nd_{(i)}$ using various crustal end-member compositions. A-type granites: TH-8, Gr1 and TH12 from Condie *et al.* (1999); lower and upper crust from Riciputi *et al.* (1995); Rock Creek lavas from Colucci *et al.* (1991) (RC^1, CoV-59b; RC^2, CoV-168v); ash-flow tuffs: FCT and CRT, Fish Canyon tuff and Carpenter Ridge tuff, respectively, from Riciputi *et al.* (1995). Italic numbers are the silica content of sample. Tick marks on curves represent the percentage of magma remaining after crystallization (10% increments).

at least two magma-evolution scenarios. The Fourmile Creek samples are distinguished from the WFSJR samples by their lower HREE + Y concentrations (Fig. 11), which require differentiation from mafic andesite to dacite through either: (1) fractional crystallization involving a mineral or minerals for which partition coefficients are $\gg$1 such as amphibole ($K_{d\ Yb}^{amph/melt} = 2{\cdot}73$; Sisson, 1994), garnet ($K_{d\ Yb}^{garnet/melt} = 53$; Irvine & Frey, 1978) and zircon ($K_{d\ Yb}^{zircon/melt} = 191$; Fujimaki, 1986); or (2) fractional crystallization and assimilation of magma or crustal material with low Y and HREE and other incompatible trace elements. Fractional crystallization of basaltic andesite with WFSJR composition (HA14), involving high proportions of amphibole and garnet, fails to adequately reproduce the required depletions of Zr because neither phase can lower Zr sufficiently (Fig. 17). Zircon fractionation could decrease the concentrations of Zr in the evolved magmas, but this model does not reproduce the low concentrations in HREE because of the low abundance of zircon required in the fractionating assemblage (Fig. 17). Thus, open-system processes again appear to be required if the evolved andesites are related to the inferred parent. Some process involving an end-member with low incompatible element contents is required. Only partial fusion of typical crustal rocks could produce Fourmile Creek silicic magmas with low Zr and low HREE contents with the requirement that zircon would be a residual phase (Watson, 1979). Low Pb isotopic ratios in Fourmile Creek andesites may reflect crustal rocks that have low Pb isotopic ratios.

Calc-alkaline lavas ranging from mafic andesite to dacite at WFSJR have well-defined compatible element trends in Harker diagrams. The best-fit crystal fractionation models for WFSJR lavas (HA14–HA18, $\Sigma r^2 = 0{\cdot}025$; Table 3) require removal of plagioclase, orthopyroxene, clinopyroxene, amphibole, magnetite and apatite, consistent with the observed phase assemblages of individual differentiation series. Although fractional crystallization was certainly involved, the large concentration ranges for incompatible elements such as Zr, LREE, Y and HREE (e.g. 119–205 ppm for Zr; twice the Ce contents at the same silica values; Fig. 11) suggest assimilation or magma mixing with an end-member characterized by low incompatible element contents. Fractional crystallization plus assimilation of surrounding ash-flow tuffs (Whitney *et al.*, 1988; Bachmann *et al.*, 2000) or crustal material (Rudnick & Fountain, 1995) cannot reproduce the low concentrations of incompatible elements in these lavas (Fig. 18). An alternative mechanism for producing the low incompatible element contents of dacite is magma mixing with an end-member with low trace element contents. Replenishment with mafic magmas may not work because of resetting to lower SiO_2 content. So except mixing between various calc-alkaline end-members, there is no single model that appears to relate all calc-alkaline magmas with each other, neither WFSJR vs Fourmile Creek magmas nor the variability

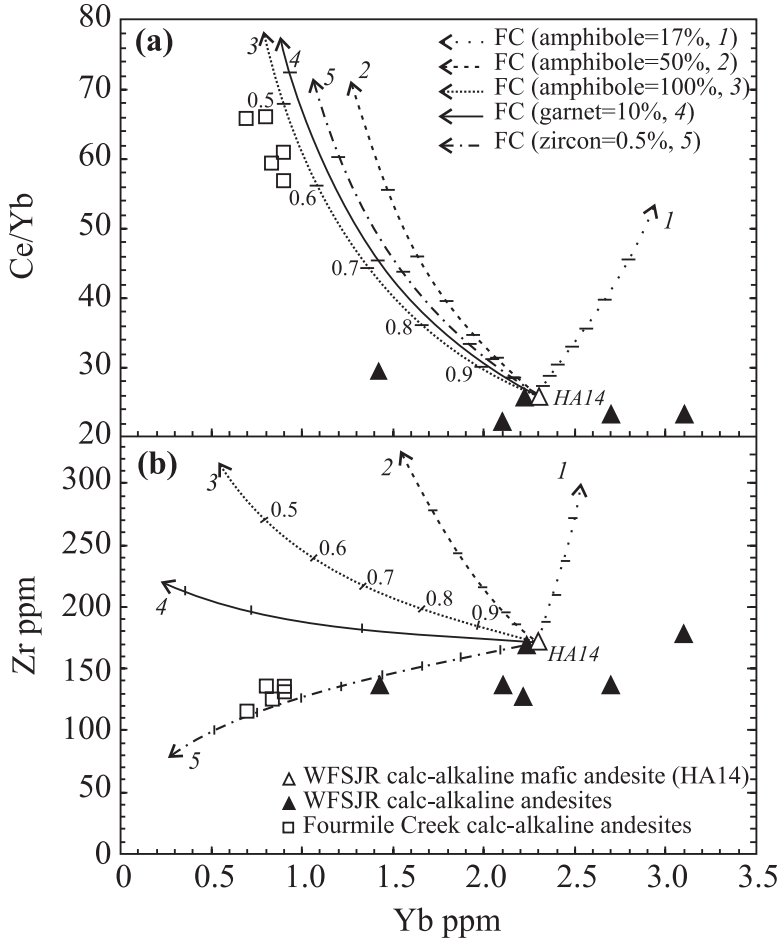

Fig. 17. (a) Ce/Yb vs Yb and (b) Zr vs Yb of calc-alkaline lavas and dykes. Dashed lines are fractional crystallization (FC) curves calculated from the less evolved lava (HA14, △), assuming fractionating assemblage of: (1) cpx_{30}, opx_{30}, $plag_{17}$, $amph_{17}$, $mag_{5·4}$ and $ap_{0·6}$; (2) $amph_{50}$, cpx_{15}, opx_{15}, $plag_{15}$, $mag_{4·4}$ and $apa_{0·6}$; (3) $amph_{100}$. Continuous and dashed curves, (4) and (5), are crystal fractionation assuming a fractionating assemblage of: (4) cpx_{25}, opx_{25}, $plag_{17}$, $amph_{17}$, $garnet_{10}$, $mag_{5·4}$, and $apa_{0·6}$; (5) cpx_{25}, opx_{25}, $plag_{22}$, $amph_{22}$, $zircon_{0·5}$, mag_5, and $apa_{0·6}$. For all curves the mineral–melt distribution coefficient for Yb in amphibole was assumed to be 2·73 (Sisson, 1994). For curves involving garnet, the mineral–melt distribution coefficients for Yb and Zr in garnet were assumed to be 53 and 0·5 (Irvine & Frey, 1978). For curves involving zircon, the mineral–melt distribution coefficient for Yb and Zr in zircon was assumed to be 191 and 254, respectively (Watson & Harrison, 1983; Fujimaki, 1986). Partition coefficients for plagioclase, pyroxene and magnetite are from Paster *et al.* (1974), Luhr & Carmichael (1980), Bacon & Druitt (1988), and Ewart & Griffin (1994). Tick marks on curves represent the percentage of magma remaining after crystallization (10% increments). WFSJR, West Fork of the San Juan River.

observed with, for example, WFSJR magmas at the higher-SiO_2 end.

Origin of the parental magmas

Depletions of HFSE relative to mantle-normalized concentrations of Rb, Ba, K and Th (Fig. 12) are widely considered to be characteristic of magmas produced above subduction zones. A critical question is whether the arc-like signature in the Huerto trace element patterns is inherited from the mantle source (e.g. Thirlwall *et al.*, 1994), or whether it reflects contamination by continental crust depleted in HFSE relative to LILE (Weaver & Tarney, 1984; Taylor & McLennan, 1995). This is particularly relevant for the San Juan volcanic field because its tectonic setting is unclear. The San Juan magmas were erupted nearly 700 km from the Oligocene trench before opening of the Rio Grande Rift and their isotopic compositions, particularly for Nd, have been interpreted in terms of substantial crustal contributions (Lipman *et al.*, 1978; Riciputi *et al.*, 1995).

Lipman *et al.* (1978) and Colucci *et al.* (1991) proposed that the andesitic magmas of the Conejos Formation resulted from lower-crustal residence and differentiation of basalt, as suggested by the low isotopic ratios of all Conejos lavas. In contrast, the Huerto trachyandesite series has relatively high Nd, Sr and Pb isotopic ratios that cannot reflect a large lower-crustal imprint. Both

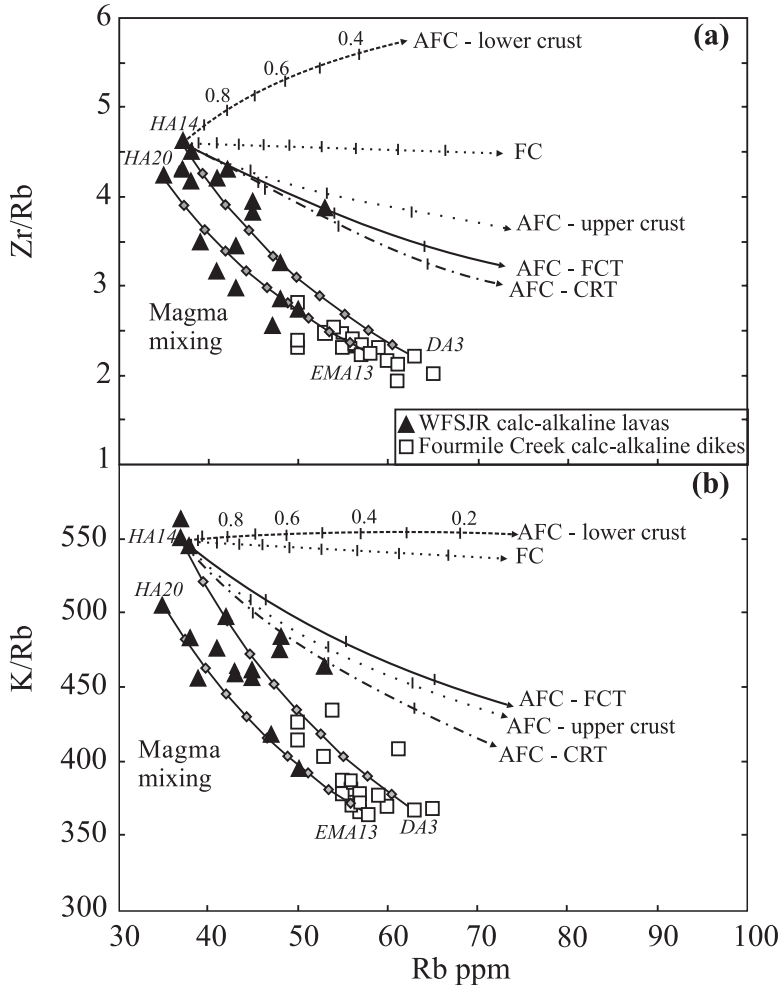

Fig. 18. (a) Zr/Rb vs Rb and (b) K/Rb vs Rb for calc-alkaline lavas and dykes and related FC and AFC modelling curves. Model curves represent closed-system crystallization (FC) and an assimilation–fractional crystallization curve (AFC) calculated after the method of DePaolo (1981). The AFC curve depicts assimilation of average lower and upper crust from Rudnick & Fountain (1995), Carpenter Ridge Tuff [CRT: LZ49 of Whitney *et al.* (1988)] and Fish Canyon Tuff [FCT: FCTpum(I) of Bachmann *et al.* (2000)] at a mass assimilation rate/crystallization rate (r) of 0·5. Mixing curves are modelled using the least evolved lavas (HA14 and HA20) and Fourmile Creek andesites (EMA13 and DA3). Tick marks on curves represent the percentage of magma remaining after crystallization (10% increments).

trachytic and calc-alkaline series have depleted HFSE relative to LILE. The differentiation from basaltic (trachy)andesite to (trachy)dacite is marked by a slight decrease in LILE/HFSE ratios (e.g. Ba/Nb is 100 to 90 for calc-alkaline series and 90 to 40 for trachyandesitic series) that may be related to oxide fractionation. The HFSE depletion may be then more probably related to the parental magma signature rather than to crustal assimilation and may be interpreted as due to a subduction origin or to a subduction-modified magma source.

The production of contemporaneous mildly alkaline and calc-alkaline lavas in the Huerto Andesite raises another question: were the parents of the trachyandesitic and calc-alkaline magmas chemically similar or different? The presence of olivine phenocrysts and relatively low silica contents in the basaltic trachyandesites suggest that their parent magmas were mantle-derived basalts. If so, two hypotheses can be considered for the derivation of the trachyandesitic and calc-alkaline lavas: (1) basaltic trachyandesites evolved from parental trachybasalts and calc-alkaline lavas, with lower total alkali and incompatible element contents, evolved from sub-alkaline parental basalts; or (2) contrasts in phase assemblages and differentiation trends reflect contrasting polybaric differentiation histories from broadly similar parental magmas (e.g. Arculus, 1976; Moore & Carmichael, 1998).

Despite the different phenocryst assemblages and the different isotopic compositions in the least evolved

magmas in the calc-alkaline and trachytic series, the apparent commonality of major and trace element compositions at 55 wt % SiO_2 as well as the similar REE patterns and elemental ratios of both series (e.g. Sr/Rb = 18·6 and 19·7, Ce/Y = 2·1 and 2·2, La/Yb = 12 and 13 for calc-alkaline mafic andesite and basaltic trachyandesite, respectively) is generally consistent with derivation from broadly similar parental magmas. The two distinct series in the Conejos Formation (Colucci *et al.*, 1991; Figs 10 and 11) also define trends that could be interpreted as indicating divergence from a common basaltic composition, but such an inference is more speculative than for the Huerto Andesite analogues because of the flatter slopes defined by trends for some elements (e.g. Ce, Fig. 11) and the much greater separation between the two Conejos magma types for others (e.g. Rb and Zr; Fig. 11). However, the large range of incompatible element concentrations around 55 wt % SiO_2 (Fig. 11) and the sparse Nd isotopic data for the Huerto Andesite (Fig. 13) do not seem to be consistent with a single parent. The range in incompatible elements may represent different degrees of melting of a single source but by the time the basaltic andesite reached crustal differentiation sites, there must have been a significant range of 'parental' magmas.

DISCUSSION

Huerto magmatism

The contrasting calc-alkaline and trachyandesitic series of the Huerto Andesite represent the third example in the San Juan volcanic field wherein andesitic magmas with different mineral assemblages, trace element signatures and isotopic compositions were erupted from broadly contemporaneous centres. Colucci *et al.* (1991) first documented these distinctions in the precaldera Conejos Formation lavas of the SW San Juan volcanic field (Horseshoe Mountain member vs Rock Creek member), and Riciputi *et al.* (1995) recognized similar distinctions between precaldera Conejos lavas of the central San Juan caldera cluster. The recurrence of the same divergent differentiation trends in the postcaldera Huerto lavas, as documented here, indicates that these trends are fundamental manifestations of San Juan magmatism. Colucci *et al.* (1991) postulated that these trends might be related to distinct mafic parent magmas: a water-rich calc-alkaline parent for the hornblende-bearing Horseshoe Mountain member and a less water-rich mildly alkaline parent for the Rock Creek member. However, they also emphasized the complicating factors of the absence of erupted basalts and strong crustal overprints on the differentiated magmas. Riciputi *et al.* (1995) further stressed the importance of open-system intracrustal differentiation. These intrinsic characteristics of San Juan volcanism render any discussion of the diversity among the basaltic precursors of San Juan andesites, or their mantle sources, highly speculative. However, the Huerto Andesite offers opportunities for resolving some uncertainties regarding parental magma character because the two differentiation series are geographically separated and they have different spatial relationships to the dominant magmatic focus of the central San Juan volcanic field. Whereas the calc-alkaline centres are located within or near the southern boundary of the La Garita caldera, within which all subsequent calderas are nested, the trachyandesitic centres are largely peripheral to it. We suggest that the trachyandesitic centres formed above crustal columns that were cooler and more dense because they were less charged with resident magmas related to large sub-caldera reservoirs.

The trachyandesitic series is relatively reduced and water poor (plagioclase + olivine + clinopyroxene + orthopyroxene + magnetite + ilmenite + F-rich apatite and sulphide) in comparison with the calc-alkaline series. The petrogenesis of trachyandesitic lavas appears mainly to reflect crystal fractionation of mantle-derived alkalic basalt, modified by assimilation of recent subvolcanic intrusions. A poorly constrained depth estimate of 1–2 kbar for evolution of the trachyandesitic series is in agreement with published phase equilibria for magmas of similar composition (Moore & Carmichael, 1998). Assuming that trachyandesitic magmas ascended through relatively dense crust to shallow levels, peripheral to the central caldera cluster, they may result from degassing of a water-rich parental basalt similar to that of the calc-alkaline lavas.

Although all calc-alkaline magmas are oxidized (>NNO + 1), wet and sulphur rich, petrographic observations and geochemical data suggest that the lavas near Fourmile Creek and WFSJR record different magmatic differentiation histories, whereas Table Mountain lavas are an erosional outlier of the WFSJR lavas (Figs 10 and 11; Christe, 2001). The differentiation path followed by the WFSJR calc-alkaline magmas requires two stages of magmatic differentiation to explain the mineralogical observations (amphibole breakdown rims, plagioclase compositions, mineral abundances and textures) and the shift from oxidized to reduced oxidation state with increasing differentiation. This two-stage history is recorded by the following assemblages: (1) An-rich plagioclase, amphibole and clinopyroxene + S-rich apatite + magnetite1 + ilmenite1 and pyrrhotite crystallized from oxidized, water- and sulphur-rich magmas; (2) upon cooling at shallower levels, the mafic andesitic to dacitic magmas crystallized dominantly plagioclase (less An-rich) + orthopyroxene + magnetite2 + ilmenite2 from a less oxidized (QFM) and probably less water- and sulphur-rich magma, and amphibole reacted to form plagioclase + pyroxenes + magnetite.

The mineralogy and bulk compositions of Fourmile Creek andesites indicate that fractionation of plagioclase + hornblende + clinopyroxene + magnetite + ilmenite + apatite + anhydrite + sulphide occurred from a more oxidized (NNO + 1·3), water- and sulphur-rich magma than the WFSJR lavas. These magmas appear to be derived from primary mantle-derived basalts, similar to the WFSJR basaltic magmas, which initially ponded in deep crustal reservoirs. Here they underwent combined fractional crystallization and lower-crustal assimilation, or mixing with crustal melts. As these eruptive centres are located inside or close to the southern part of La Garita caldera, the calc-alkaline magmas may have risen directly below the felsic magma chambers. Because of decreasing crustal density induced by voluminous focused felsic magmatism they may have been trapped beneath the central caldera cluster before reaching the surface and probably, in places, they may have interacted with already evolved WFSJR magmas.

Implications for magma genesis in the Central San Juan volcanic field

Huerto volcanism is typical of the andesitic activity that occurred within and around many San Juan calderas between large silicic ash-flow tuff eruptions. Erupted just after the Fish Canyon Tuff (28·0 Ma, >5000 km^3), the Huerto Andesite is likely to be the extrusive equivalent of water-rich intrusions that were responsible for rejuvenating and remobilizing the shallow (2·4 kbar; Johnson & Rutherford, 1989) and partly solidified subcaldera plutons from which the Fish Canyon Tuff was generated prior to eruption (Bachmann & Bergantz, 2003). Generation of the Fish Canyon dacitic magma almost certainly was accompanied by hybridization of the crustal column beneath the central San Juan caldera cluster (Lipman *et al.*, 1978; Riciputi *et al.*, 1995). These modifications would have favoured deeper emplacement of mafic to intermediate magmas intruded directly into the subcaldera column than would have been the case for magmatic systems peripheral to the main focus. The inability of mafic magmas to ascend through less dense crust or resident intrusions of low-density silicic magma (e.g. Cox, 1980) would favour the ponding of the mafic calc-alkaline magmas within or at the base of the lower crust. We favour such a scenario for the volatile retention that led to the hornblende-bearing calc-alkaline Huerto magmas, although there is good evidence that these magmas underwent pre-eruptive degassing that led to partial breakdown of hornblende phenocrysts and a shift to less oxidizing conditions in the more evolved calc-alkaline magmas.

All Huerto andesites attest to a strong imprint of crustal components. However, the occurrence of trachyandesitic lavas without a lower-crustal imprint and with a subduction-related geochemical signature argues for an origin from subduction-modified sources for magmas of the San Juan volcanic field. The Huerto Andesite represents another case of contemporaneous trachyandesitic and calc-alkaline lavas that are essentially described in subduction-related volcanoes (e.g. Arculus, 1976; Luhr & Carmichael, 1982; Nelson & Livieres, 1986; Luhr, 1992). Furthermore, the occurrence of sulphides in the trachyandesitic and WFSJR calc-alkaline lavas and anhydrite + pyrrhotite in the Fourmile Creek dykes (Parat *et al.*, 2002) points to initially sulphur-rich magmas in both series. All other recognized examples of sulphur-rich magmas are subduction related (e.g. Carroll & Rutherford, 1988; Rutherford & Devine, 1996; Kress, 1997). Although the Oligocene geodynamic setting of the San Juan volcanic field is far from clear, particularly with respect to whether or not San Juan magmatism was a direct consequence of concurrent subduction, these Oligocene andesitic magmas are in most ways indistinguishable from magmas erupted in many currently active volcanic arcs.

ACKNOWLEDGEMENTS

We are grateful to A. Marzoli and F. Costa for useful discussions, and to M. Pichavant and B. Scaillet for making available their unpublished experimental data. We thank M. Mamberti for ICP-MS analyses, F. Caponi for XRF analyses, P. Voldet for ICP-AES analyses, and D. Fontignie and M. Chiaradia for isotope analyses. Reviews by M. Streck, C. Bacon and the editor M. Wilson considerably improved the manuscript. This study was supported by the Immanuel Friedlander Foundation and Swiss Fonds National Grant 20-49730.96 to M.A.D.

SUPPLEMENTARY DATA

Supplementary data for this paper are available on *Journal of Petrology* online.

REFERENCES

Arculus, R. J. (1976). Geology and geochemistry of the alkali basalt–andesite association of Grenada, Lesser Antilles island arc. *Geological Society of America Bulletin* **87**(4), 612–624.

Askren, D. R., Whitney, J. A. & Roden, M. F. (1991). Petrology and geochemistry of the Huerto Andesite, San Juan volcanic field, Colorado. *Contributions to Mineralogy and Petrology* **107**, 373–386.

Bachmann, O. & Bergantz, G. W. (2003). Rejuvenisation of the Fish Canyon magma body: a window into the evolution of large-volume silicic magma systems. *Geology* **31**(9), 789–792.

Bachmann, O., Dungan, M. A. & Lipman, P. W. (2000). Voluminous lava-like precursor to a major ash-flow tuff; low-column pyroclastic

eruption of the Pagosa Peak Dacite, San Juan volcanic field, Colorado. *Journal of Volcanology and Geothermal Research* **98**(1–4), 153–171.

Bachmann, O., Dungan, M. A. & Lipman, P. W. (2002). The Fish Canyon magma body, San Juan volcanic field, Colorado: rejuvenation and eruption of an upper-crustal batholith. *Journal of Petrology* **43**(8), 1469–1503.

Bacon, C. R. & Druitt, T. H. (1988). Compositional evolution of the zoned calc-alkaline magma chamber of Mount Mazama, Crater Lake, Oregon. *Contributions to Mineralogy and Petrology* **98**(2), 224–256.

Bacon, C. R. & Hirschmann, M. M. (1988). Mg/Mn partitioning as a test for equilibrium between coexisting Fe–Ti oxides. *American Mineralogist* **73**, 57–61.

Baker, D. R. & Eggler, D. H. (1987). Compositions of anhydrous and hydrous melts coexisting with plagioclase, augite and olivine or low-Ca pyroxene from 1 atm to 8 kbar: application to the Aleutian volcanic center of Atka. *American Mineralogist* **72**, 12–28.

Barrat, J. A., Keller, F., Amosse, J., Taylor, R. N., Nesbitt, R. W. & Hirata, T. (1996). Determination of rare earth elements in sixteen silicate reference samples by ICP-MS after Tm addition and ion exchange separation. *Geostandards Newsletter* **20**(1), 133–139.

Boynton, W. V. (1984). Cosmochemistry of the rare earth elements; meteorite studies. In: Henderson, P. (ed.) *Rare Earth Element Geochemistry*. Amsterdam: Elsevier, pp. 63–114.

Carroll, M. R. & Rutherford, M. J. (1987). The stability of igneous anhydrite: experimental results and implications for sulphur behavior in the 1982 El Chichón trachyandesite and other evolved magmas. *Journal of Petrology* **28**, 781–801.

Carroll, M. R. & Rutherford, M. J. (1988). Sulphur speciation in hydrous experimental glasses of varying oxidation states: results from measured wavelength shifts of sulphur X-rays. *American Mineralogist* **73**, 845–849.

Chiaradia, M. & Fontboté, L. (2003). Separate lead isotope analyses of leachate and residue rock fractions: implications for metal source tracing. *Mineralium Deposita* **38**, 185–195.

Christe, P. (2001). Petrology and geochemistry of the Table Mountain lavas, San Juan Volcanic Field, Colorado, U.S.A: hornblende-rich andesites and their role in the late-stage evolution of a silicic igneous system. Diploma thesis, Basel, 81 pp.

Colucci, M. T., Dungan, M. A. & Ferguson, K. M. (1991). Precaldera lavas of the southeast San Juan volcanic field: parent magmas and crustal interactions. *Journal of Geophysical Research* **96**(B8), 13413–13434.

Condie, K. C., Latysh, N., Van Schmus, W. R., Kozuch, M. & Selverstone, J. (1999). Geochemistry, Nd and Sr isotopes, and U/Pb zircon ages of granitoid and metasedimentary xenoliths from the Navajo volcanic field, Four Corners area, Southwestern United States. *Chemical Geology* **156**(1–4), 95–133.

Coney, P. J. & Reynolds, S. J. (1977). Cordilleran Benioff zones. *Nature* **270**(5636), 403–406.

Cox, K. G. (1980). A model for flood basalt volcanism. *Journal of Petrology* **21**(4), 629–650.

Deer, W. A., Howie, R. A. & Zussman, J. (1992). *An Introduction to the Rock-forming Minerals*. Harlow: Longman, 696 pp.

DePaolo, D. J. (1981). Trace element and isotopic effects of combined wallrock assimilation and fractional crystallization. *Earth and Planetary Science Letters* **53**(2), 189–202.

Dorais, M. J., Whitney, J. A. & Stormer, J. C., Jr (1991). Mineralogical constraints on the petrogenesis of trachytic inclusions, Carpenter Ridge Tuff, central San Juan volcanic field, Colorado. *Contributions to Mineralogy and Petrology* **107**(2), 219–230.

Eggler, D. H. & Burnham, C. W. (1973). Crystallization and fractionation trends in system andesite–H_2O–CO_2–O_2 at pressures to 10 Kb. *Geological Society of America Bulletin* **84**(8), 2517–2532.

Evans, B. W. & Scaillet, B. (1997). The redox state of Pinatubo dacite and ilmenite–hematite solvus. *American Mineralogist* **82**, 625–629.

Ewart, A. & Griffin, W. L. (1994). Application of proton-microprobe data to trace-element partitioning in volcanic rocks. *Chemical Geology* **117**(1–4), 251–284.

Fujimaki, H. (1986). Partition coefficients of Hf, Zr, and REE between zircon, apatite, and liquid. *Contributions to Mineralogy and Petrology* **94**(1), 42–45.

Gaetani, G. A., Grove, T. L. & Bryan, W. B. (1993). The influence of water on the petrogenesis of subduction-related igneous rocks. *Nature* **365**(6444), 332–334.

Ghiorso, M. S. & Sack, R. O. (1991). Fe–Ti oxide geothermometry: thermodynamic formulation and the estimation of intensive variables in silicic magmas. *Contributions to Mineralogy and Petrology* **108**, 485–510.

Grove, T. L. & Kinzler, R. J. (1986). Petrogenesis of andesites. *Annual Review of Earth and Planetary Sciences* **14**, 417–454.

Grove, T. L., Gerlach, D. C. & Sando, T. W. (1982). Origin of calc-alkaline series lavas at Medicine Lake volcano by fractionation, assimilation and mixing. *Contributions to Mineralogy and Petrology* **80**, 160–182.

Harrison, T. M. & Watson, E. B. (1984). The behavior of apatite during crustal anatexis: equilibrium and kinetic considerations. *Geochimica et Cosmochimica Acta* **48**, 1467–1477.

Hibbard, M. J. (1981). The magma mixing origin of mantled feldspars. *Contributions to Mineralogy and Petrology* **76**, 158–170.

Irvine, A. J. & Frey, F. A. (1978). Distribution of trace elements between garnet megacrysts and host volcanic liquids of kimberlitic to rhyolitic composition. *Geochimica et Cosmochimica Acta* **42**, 771–787.

Johnson, M. C. & Rutherford, M. J. (1989). Experimentally determined conditions in the Fish Canyon Tuff, Colorado, magma chamber. *Journal of Petrology* **30**(3), 711–737.

Kress, V. (1997). Magma mixing as a source for Pinatubo sulphur. *Nature* **389**, 591–593.

Larsen, E. S. & Cross, W. (1956). *Geology and Petrology of the San Juan Region, Southwestern Colorado. US Geological Survey Professional Paper* **258**, 303 pp.

Latysh, N. (1997). Geochemistry and origin of the granitoid xenoliths from the Navajo volcanic field, Four Corners Area, SW United States. Ph.D. thesis, New Mexico Institute of Mining and Technology, Socorro.

Leake, B. E., Woolley, A. R., Arps, C. E. S., *et al.* (1997). Nomenclature of amphiboles: report of the subcommittee on amphiboles of the International Mineralogical Association, commission on new minerals and mineral names. *American Mineralogist* **82**, 1019–1037.

Le Bas, M. J., Le Maitre, R. W., Streckeisen, A. & Zanettin, B. (1986). A chemical classification of volcanic rocks based on the total alkali–silica diagram. *Journal of Petrology* **27**(3), 745–750.

Lindsley, D. H. (1983). Pyroxene thermometry. *American Mineralogist* **68**, 477–493.

Lindsley, D. H. & Frost, B. R. (1992). Equilibria among Fe–Ti oxides, pyroxenes, olivine, and quartz: Part I. Theory. *American Mineralogist* **77**, 987–1003.

Lipman, P. W. (1975). *Evolution of the Platoro Caldera Complex and Related Volcanic Rocks, Southeastern San Juan Mountains, Colorado. US Geological Survey Professional Paper* **852**, 128 pp.

Lipman, P. W. (2000). The central San Juan caldera cluster: regional volcanic framework. In: Bethke, P. M. & Hay, R. L. (eds) *Ancient Lake Creede: Its Volcano-Tectonic Setting, History of Sedimentation and Relation to Mineralization in the Creede Mining District. Geological Society of America, Special Papers* **346**, 9–69.

Lipman, P. W. (2004). *Geologic Map of the Central San Juan Caldera Cluster, Southwestern Colorado. US Geological Survey Miscellaneous Investigations Map* **I-2799**.

Lipman, P. W., Steven, T. A. & Mehnert, H. H. (1970). Volcanic history of the San Juan Mountains, Colorado, as indicated by potassium–argon dating. *Geological Society of America Bulletin* **81**, 2327–2352.

Lipman, P. W., Prostka, H. J. & Christiansen, R. L. (1972). Cenozoic volcanism and plate-tectonic evolution of the western United States, I, Early and middle Cenozoic. *Philosophical Transactions of the Royal Society of London, Series A* **271**, 217–248.

Lipman, P. W., Doe, B. R., Hedge, C. E. & Steven, T. A. (1978). Petrologic evolution of the San Juan volcanic field, southwestern Colorado; Pb and Sr isotope evidence. *Geological Society of America Bulletin* **89**(1), 59–82.

Lipman, P. W., Dungan, M. A. & Bachmann, O. (1997). Comagmatic granophyric granite in the Fish Canyon Tuff, Colorado: implications for magma-chamber processes during a large ash-flow eruption. *Geology* **25**(10), 915–918.

Luhr, J. F. (1990). Experimental phase relations of water- and sulphur-saturated arc magmas and the 1982 eruption of El Chichón n volcano. *Journal of Petrology* **31**, 1071–1114.

Luhr, J. F. (1992). Slab-derived fluids and partial melting in subduction zones; insights from two contrasting Mexican volcanoes (Colima and Ceboruco). *Journal of Volcanology and Geothermal Research* **54**(1–2), 1–18.

Luhr, J. F. & Carmichael, I. S. E. (1980). The Colima Volcanic complex, Mexico. I. Post-caldera andesites from Volcan Colima. *Contributions to Mineralogy and Petrology* **71**, 343–372.

Luhr, J. F. & Carmichael, I. S. E. (1982). The Colima volcanic complex, Mexico III, Ash- and scoria-fall deposits from the upper slopes of Volcan Colima. *Contributions to Mineralogy and Petrology* **80**, 262–275.

Miyashiro, A. (1974). Volcanic rock series in island arcs and active continental margins. *American Journal of Science* **274**(4), 321–355.

Moore, G. & Carmichael, I. S. E. (1998). The hydrous phase equilibria (to 3 kbar) of an andesite and basaltic andesite from western Mexico: constraints on water content and conditions of phenocryst growth. *Contributions to Mineralogy and Petrology* **130**, 304–319.

Morimoto, N., Fabries, J., Ferguson, A. K., *et al.* (1988). Nomenclature of pyroxenes. *American Mineralogist* **73**(9–10), 1123–1133.

Nelson, S. A. & Livieres, R. A. (1986). Contemporaneous calc-alkaline and alkaline volcanism at Sanganguey Volcano, Nayarit, Mexico. *Geological Society of America Bulletin* **97**(7), 798–808.

Parat, F., Dungan, M. A. & Streck, M. J. (2002). Anhydrite, pyrrhotite and sulphur-rich apatite: tracing the sulphur evolution of an Oligocene andesite (Eagle Mountain, Colorado, U.S.A.). *Lithos* **64**, 63–75.

Paster, T. P., Schauwecker, D. S. & Haskin, L. A. (1974). The behavior of some trace elements during solidification of the Skaergaard layered series. *Geochimica et Cosmochimica Acta* **38**(10), 1549–1577.

Peacock, M. A. (1931). Classification of igneous rocks series. *Journal of Geology* **39**, 54–67.

Pichavant, M., Martel, C., Bourdier, J.-L. & Scaillet, B. (2002). Physical conditions, structure, and dynamics of a zoned magma chamber: Mont Pelée (Martinique, Lesser Antilles Arc). *Journal of Geophysical Research—Solid Earth* **107**(B5), 2093, doi: 10.1029/2001JB000315.

Ratté, J. C. & Steven, T. A. (1967). *Ash Flows and Related Volcanic Rocks Associated with the Creede Caldera, San Juan Mountains, Colorado. US Geological Survey Professional Paper* **524-H**, 58 pp.

Rhodes, J. M. (1988). Geochemistry of the 1984 Mauna Loa eruption: implications for magma storage and supply. *Journal of Geophysical Research* **93**, 4453–4466.

Riciputi, L. R. (1991). Petrology and Nd, Sr and Pb isotopes of the central San Juan caldera cluster, Colorado. Ph.D. thesis, University of Wisconsin, Madison.

Riciputi, L. R., Johnson, C. M., Sawyer, D. A. & Lipman, P. W. (1995). Crustal and magmatic evolution in a large multicyclic caldera complex: isotopic evidence from the central San Juan volcanic field. *Journal of Volcanology and Geothermal Research* **67**, 1–28.

Rollinson, H. (1993). *Using Geochemical Data: Evaluation, Presentation, Interpretation*. Singapore: Longman, 352 pp.

Rudnick, R. L. & Fountain, D. M. (1995). Nature and composition of the continental crust; a lower crustal perspective. *Reviews of Geophysics* **33**(3), 267–309.

Rutherford, M. J. & Devine, J. D. (1996). Pre-eruption pressure–temperature conditions and volatiles in the 1991 dacitic magma of Mount Pinatubo. In: Newhall, C. G. & Punongbayan, R. S. (eds) *Fire and Mud. Eruptions and Lahars of Mount Pinatubo, Philippines*. Seattle, WA: University of Washington Press, pp. 751–766.

Rutherford, M. J. & Hill, P. M. (1993). Magma ascent rates from amphibole breakdown: an experimental study applied to the 1980–1986 Mount St. Helens eruptions. *Journal of Geophysical Research* **98**(B11), 19667–19685.

Scaillet, B. & Evans, B. W. (1999). The 15 June 1991 eruption of Mount Pinatubo. I. Phase equilibria and pre-eruption P–T–fO_2–fH_2O conditions of the dacite magma. *Journal of Petrology* **40**(3), 381–411.

Schilling, J. G., Hanan, B. B., McCully, B., Kingsley, R. H. & Fontignie, D. (1994). Influence of the Sierra Leone mantle plume on the equatorial Mid-Atlantic Ridge: a Nd–Sr–Pb isotopic study. *Journal of Geophysical Research* **99**, 12005–12028.

Silver, L. T. & McGetchin, T. R. (1994). Observations on the nature of the Precambrian crust under the southern Colorado Plateau. *Geological Society of America, Abstracts with Programs* **26**(6), 63.

Sisson, T. W. (1994). Hornblende–melt trace-element partitioning measured by ion microprobe. Trace-element partitioning with application to magmatic processes. *Chemical Geology* **117**(1–4), 331–344.

Sisson, T. W. & Grove, T. L. (1993). Experimental investigations of the role of H_2O in calc-alkaline differentiation and subduction zone magmatism. *Contributions to Mineralogy and Petrology* **113**, 143–166.

Smith, J. V. & Brown, W. L. (1988). *Feldspar Minerals. 1. Crystal Structures, Physical, Chemical and Microtextural Properties*. Berlin: Springer, 828 pp.

Stein, H. J. (1985). A lead, strontium, and sulphur isotope study of Laramide–Tertiary intrusions and mineralization in the Colorado Mineral Belt with emphasis of Climax-type porphyry molybdenum systems plus a summary of newly acquired isotopic and rare earth element data. Ph.D. thesis, University of North Carolina, Chapel Hill.

Steven, T. A. & Lipman, P. W. (1976). *Calderas of the San Juan Volcanic Field, Southwestern Colorado. US Geological Survey Professional Paper* **958**, 1–35.

Steven, T. A., Lipman, P. W. & Olson, J. C. (1974). Ash-flow stratigraphy and caldera structures in the San Juan volcanic field, southwestern Colorado. *US Geological Survey Bulletin* **394-A**, A75–A82.

Stormer, J. C. (1983). The effects of recalculation on estimates of temperature and oxygen fugacity from analyses of multicomponent iron–titanium oxides. *American Mineralogist* **68**, 586–594.

Sun, S. S. & McDonough, W. F. (1989). Chemical and isotopic systematics of oceanic basalts; implications for mantle composition and processes. In: Saunders, A. D. & Norry, M. J. (eds) *Magmatism in the Ocean Basins. Geological Society, London, Special Publications* **42**, 313–345.

Taylor, S. R. & McLennan, S. M. (1995). The geochemical evolution of the continental crust. *Reviews of Geophysics* **33**(2), 241–265.

Thirlwall, M. F., Smith, T. E., Graham, A. M., Theodorou, N., Hollings, P., Davidson, J. P. & Arculus, R. J. (1994). High field strength element anomalies in arc lavas; source or process? *Journal of Petrology* **35**(3), 819–838.

Voldet, P. (1993). From neutron activation to inductively coupled plasma-atomic emission spectrometry in the determination of rare-earth elements in rocks. *Trends in Analytical Chemistry* **12**, 339–344.

Watson, E. B. (1979). Zircon saturation in felsic liquids; experimental results and applications to trace element geochemistry. *Contributions to Mineralogy and Petrology* **70**(4), 407–419.

Watson, E. B. & Harrison, T. M. (1983). Zircon saturation revisited; temperature and composition effects in a variety of crustal magma types. *Earth and Planetary Science Letters* **64**(2), 295–304.

Weaver, B. L. & Tarney, J. (1984). Empirical approach to estimating the composition of the continental crust. *Nature* **310**(5978), 575–577.

Whitney, J. A. & Stormer, J. C. (1985). Mineralogy, petrology, and magmatic conditions from the Fish Canyon Tuff, Central San Juan volcanic field, Colorado. *Journal of Petrology* **26**(3), 726–762.

Whitney, J. A., Dorais, M. J., Stormer, J. C., Jr, Kline, S. W. & Matty, D. J. (1988). Magmatic conditions and development of chemical zonation in the Carpenter Ridge Tuff, central San Juan volcanic field, Colorado. *American Journal of Science* **288-A**, 16–44.

Yager, D. B., Lipman, P. W. & Sawyer, D. A. (1991). Caldera-related lavas and intrusion of the south–central San Juan Mountains, Colorado—analytical data. *US Geological Survey Open-File Report* **91-313**, 19 pp.